This is to certify that the
thesis entitled

CMOS INSTRUMENTATION FOR ON-CHIP

BIOFLUORESCENCE AND

BIOELECTROCHEMICAL ASSAYS

presented by

WAQAR AHMED QURESHI

has been accepted towards fulfillment
of the requirements for the

M.S degree in ELECTRICAL ENGINEERING

Major Professor's Signature

August 13, 2010

Date

MSU is an Affirmative Action/Equal Opportunity Employer

CMOS INSTRUMENTATION FOR ON-CHIP BIOFLUOROSCENCE AND BIOELECTROCHEMICAL ASSAYS

By

Waqar Ahmed Qureshi

A THESIS

Submitted to
Michigan State University
In partial fulfillment to the requirements
for the degree of

MASTER OF SCIENCE

Electrical Engineering

2010

ABSTRACT

CMOS INSTRUMENTATION FOR ON-CHIP BIOFLUOROSCENCE AND BIOELECTROCHEMICAL ASSAYS

By

Waqar Ahmed Qureshi

Membrane proteins embedded in bilayer lipid membranes (BLM) play a vital role in biological functions. The molecular mechanisms by which these nanostructured bio-interfaces efficiently perform many critical tasks are poorly understood. Thus, there is a pressing need for advanced tools to measure structural and functional properties of bio-interfaces for applications including proteomics, drug screening and nanosafety. Transduction techniques including electrochemical, optical and thermal methods are widely used for bio-interface characterization. However, biological understanding could be greatly improved by a versatile instrumentation system capable of performing multiple characterization methods simultaneously. This dissertation addresses challenges to combining optical and electrochemical detection schemes on a monolithic chip in order to simultaneously monitor both structural characteristics and functional activities. Several possible architectures for electrochemical amperometry and optical measurement were analyzed, and key challenges in integrating these methods were identified. A multi-mode voltammetry CMOS instrumentation chip tailored to BLM interfaces was developed. For optical detection, a CMOS imager array suitable for a combined opto-electrochemical system was developed with a novel on-chip optical filter utilizing CMOS metal layers. The results of this research lay a solid foundation for the future implementation of a fully integrated opto-electrochemical detection system.

To my parents and my (late) sister

ACKNOWLEDGMENTS

All glory be to the most praiseworthy who showered His countless blessings on me throughout the span of my life. With the prolific praise of the Owner of Honor, I desire to begin a limitless praise, with which He is pleased and I cite His own words; *"All praise to Allah, the Lord of the worlds"*. **The Quran (39:75).**

I am honored to have one of the most distinguished scholars, Professor Andrew.J. Mason, as my advisor. I would like to thank him for his support throughout my stay at MSU. I found him an extremely intelligent researcher, exceptionally intellectual advisor and an excellent teacher. This work could not have been possible without his ever critical attitude towards my neophyte research ideas, followed by his tremendous encouragement to heighten my confidence.

I am obliged to my family, especially my parents, for their selfless support throughout my life, and particularly during the span of this work. I am running short on words to express my sentiments towards my parents for their gracious deeds and self-sacrificing exertions to empower my advancement. Accomplishment of this work is an implicit consequence of my Fathers vigorous attitude to boost my motivation and enthusiasm, and my Mothers affectionate prayers. I am also thankful to my other family members including my brothers and sister for their unbounded yet unconditional love, and having absolute faith in me.

Life in the US could not have been easier in the absence of steadfast friends and wonderful colleagues and they deserve a special mention here. Stating in alphabetical v order, I found companions like Ahmed, Awais, Brig. Qaiser, Hassan

Aqeel, Jawad, Khawar, Maaz, Sajjad zaidi, Shahzad, Tariq Abdul-Rehman, and Zubair who kept my morale high and made my stay a superb experience, here at MSU.

Advanced Microsystems and Circuits lab (AMSAC), leaded by Prof. Mason, is a fantastic team exploring the cutting-edge research. I am proud to be a part of it. I am grateful to Daniel Rairigh, Xioayi Mu, Xiaowen Liu, Li Haitao, Li Lin, Yue Huang and Yuning for their help and support. It is my pleasure to know and work with them.

Lastly I want to extend my gratitude to my advisory committee members, Professor Shantanu Chakrabartty and Professor Michael Shanblatt, for their uninterrupted patronization during the course of this work. Their extensive feedbacks not only opened new horizons of research for me, but also endowed me with insights into intricate engineering concepts. I am fortunate to have their persistent contribution and involvement in my work.

Table of Contents

List of Tables

List of Figures

Images in thesis are presented in color.

Chapter 1
Introduction

1.1 Overview of Biosensors

1.1.1 Introduction

Biosensors play an important role in our daily lives through healthcare, environmental analysis and industrial process controls. Recent advances in sensor technologies and microelectronics have resulted in a rapid growth in the development of new biomaterials such as conducting polymers, copolymers and sol gels, and many improvements in sensing techniques resulting in miniaturized and portable instruments have been reported. The potential growth in the biosensor industry is significant and is becoming one of the fastest growing sectors in the world. New analysis from Frost & Sullivan, World Biosensors Markets, reveals that the biosensor market is expected to grow from $6.72 billion in 2009 to $14.42 billion in 2016. The main reason for this fast growth is the breadth and depth at which biosensor technology has been increasingly applied to both medical and non-medical applications. A major part of biosensor revenue is due to applications in health care and clinical diagnostics, especially in "glucose testing".

1.1.2 Definitions

A **biosensor** is commonly defined as an analytical device that uses a biological recognition system to identify molecules and macromolecules. Typically biosensors are comprised of three components, as shown in Figure.1: (1) the **detector**, which is a biological sensing element that gives a response to only the specified target analyte, (2) the **transducer**, which converts the detector response

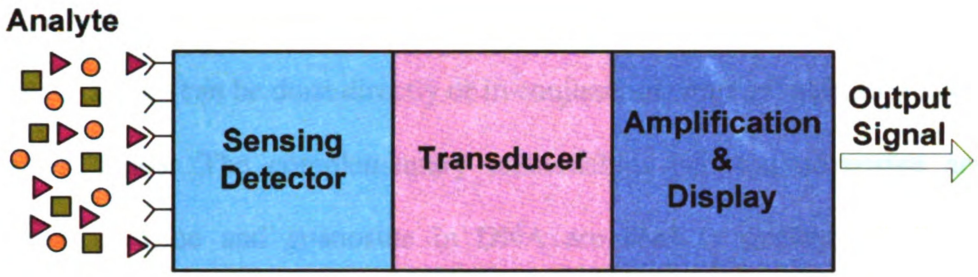

Figure 1.1 Main components of biosensor.

into a useful (generally optical or electrical) output signal; and (3) **the output system**, which involves amplification,

filtering, signal processing, and display of the output in an appropriate format. The detector typically may be an enzyme, an antibody, a receptor or a cell. The performance of biosensors is characterized by its speed, sensitivity, accuracy and portability.

1.1.3 Classes of Biosensors

Biosensors can be classified either by the type of biological sensing element they utilize or by the method employed for detection and transduction [1]. Common biological sensing elements and transduction methods are summarized below.

1.1.3.1 Biological sensing elements

(a) Antibody/antigen (Ab/Ag): The non-covalent antibody-antigen interaction is similar to a "lock" and "key" effect between an enzyme and a substrate. This exact and specific interaction is used for detection, identification and measurement of target molecules[2, 3]. This interaction can be detected either through fluorescent labeling or by observing a refractive index or reflectivity change [4].

(b) Enzymes: Enzyme-based biosensors operate either by producing or consuming a protein and/or some electroactive species. Based on their binding

capabilities and catalytic activity, enzymes are used for specific detection and measurement, which can be done directly or in conjunction with an indicator [2, 4].

(c) **Nucleic acids:** The complementary relationships between adenosine and thymine and cytosine and guanosine in DNA are used in nucleic acid-based biosensors to identify small concentrations of DNA in large samples. This identification is done by comparing a DNA sample with DNA of known organism also called DNA probe [5].

(d) **Cells and viruses:** Microorganisms such as bacteria and fungi are used as biosensors to detect specific molecules or the overall "state" of the surrounding environment and have been used in the development of biosensors and biochips [2]. Biosensors based on these engineered bacteria are used to detect stress conditions, toxicity or DNA damaging agents and other specific organic and non-organic compounds [6]. Also cellular biosensors are used for testing and monitoring the effectiveness of drugs and therapies [7].

(e) **Biomimetic materials based:** A biomimetic biosensor is an artificial or synthetic sensor that is fabricated and designed to mimic the function of a natural biosensor[2]. Several different technologies including genetic engineering of molecules, artificial cell membrane fabrication, and molecular imprinting have been developed to construct these biomimetic receptors [8-12].

1.1.3.2 Methods of Transduction

Based on the method of signal transduction and detection biosensors can be classified into following categories [2, 13].

(a) Optical Detection: Optical detection biosensors are the most diverse class of biosensors and can be used for many different types of spectroscopy, such as absorption, fluorescence, chemiluminescence, RAMAN, SERS, refraction and dispersion spectrometry [14-18]. These techniques are usually used to measure different properties, such as energy, amplitude, polarization, phase and detection time.

(b) Electrochemical Detection: Electrochemical detection provides another possible means of transduction [19-29] and electrochemical biosensors are designed to measure the current produced from reduction-oxidation (redox) reactions. The resulting current produced is directly correlated to the bulk concentration of electroactive species present or its production/consumption rate [5].

(c) Mass-sensitive: These biosensors are used to detect small changes in the mass of and interface due to chemical binding of target analytes. The mass changes are commonly measured indirectly through a change in oscillation frequency of a resonating crystal [5].

(d) Thermal Detection: Thermal biosensors measure the changes in temperature in the reaction between an enzyme molecule and a suitable analyte. These changes in temperature translate to the amount of reactants consumed or products formed [30].

1.1.4 Advantages

Biosensors promise significant advantages over non-biological sensing technologies. First, biosensors exhibit impressive sensitivity because biomolecules often possess high affinity toward their targets [31]. For example, antibodies capture antigens with a dissociation constant at the nanomolar scale, and DNA-

DNA interactions are even stronger than those of antigen-antibody [32]. Secondly, biological recognition is usually very selective because most biosensors only react in the presence of the target analyte. Moreover, due to advances in modern electronics especially CMOS technology, it has become possible to develop inexpensive, integrated, portable and ready-to-use miniaturized biosensor devices. Miniaturized biological sensors improve the ability to detect pathogens or perform genetic analysis in hospitals; more importantly, they are particularly useful for small clinics and point-of care analysis.

In today's world of rapid information access, miniaturized biosensors can serve exceptionally well in emergency situations or for on-site field applications. Typically, the smaller the device, the faster and more sensitive the response is. In most cases, biosensors can easily detect analytes in the micromolar to picomolar range [33-37].

Ease-of-use and reduced labor requirements provide additional advantages of miniaturized biosensors as compared to other traditional techniques such as atomic absorption spectrometry, inductively coupled atomic electron spectrometry, and sequential extraction procedure. The results obtained from miniaturized biosensors are compatible with and comparable to chemical analysis, while being free of chemical extractions and analytical procedures [38].

1.1.5 Applications

There is an increasing demand for inexpensive and reliable sensors to allow not only routine monitoring in a central or satellite laboratory but also analysis with greater patient contact, such as in a hospital ward, emergency room, or operating

room. Biosensors play a major role in our daily lives in a wide number of applications including healthcare and biomedical diagnostics, environmental monitoring, industrial process control, and military purposes. In healthcare, biosensors are used to measure metabolites, ions, blood oxygen, and many other parameters; to monitor patients during intensive care and surgery; and to investigate genetic disorders [39, 40]. In environmental monitoring biosensors monitor the efficacy of physical, chemical or biological pollution and measure toxic chemicals and analytes resulting from biochemical and chemical transformations [41]. Biosensors are also used in industrial process control to improve product quality, increase product yield, improve plant performance, reduce raw materials and optimize energy. Biosensors are used in the creation of bio-fuel alternative energy sources. They are also critical for detection and warning of chemical or biological agents in warfare and civilian security.

1.2 Membrane-protein-based biosensors

1.2.1 Motivation

Proteins embedded in bilayer lipid membranes (BLM) play a vital role in biological functions and are highly useful because of their unique roles in cellular function and drug discovery [42]. These nanostructured membrane proteins are used for the transport of substances across membranes, enzymatic activity, intracellular joining, recognition of other cells and signal transduction. Physical and chemical properties of membrane proteins need to be better understood because they dictate the molecular mechanisms by which membranes perform their cellular functions. To study these mechanisms, new biosensors are needed to characterize the multi-

protein membrane complexes that are regulated by a wide range of interacting partners. Such protein array biosensors are highly desired for preclinical, toxicological and clinical studies in order to ascertain candidates for drug screening, monitor efficacy and toxicity, and identify diagnostic markers. Despite the critical need to monitor membrane protein activities, the existing tools and techniques are too time consuming, labor intensive and expensive to permit wide-spread application and high-throughput operation.

Several labeled and label-free detection techniques are currently used to measure the multiple activities and characteristics of membrane proteins. Some of these are measured by optical detection schemes e.g. fluorescence, bioluminescence. Some are measured by electrochemical detection schemes, e.g. voltammetry and impedance spectroscopy, which have the advantage of direct transduction to electrical data, being less prone to interference, and the potential to miniaturize the entire measurement system [43]. An instrumentation system to measure the activities and characteristics of membrane proteins must include multiple detection schemes and ideally incorporate both optical and electrochemical methods.

1.2.2 Advantages of Microsystem

Sensitivity and portability are among the most demanding requirements for miniaturized biosensors. The rapid development of microelectronics technologies has created many opportunities to develop highly integrated, on-chip, electrical biosensors with many advantages in terms of sensitivity, quantification and accuracy. Many semiconductor devices and fabrication processes exhibit high

compatibility with biological materials that has enabled the expanding use of microelectronic and MEMS devices to integrate a large number of biological recognition elements within a single package to form integrated microsystems. The high level of integration results in enhancing the functionality and provides substantial parallelism that enables high throughput. On-chip biosensors facilitate miniaturized, low power, hand-held and portable instrumentation systems that are vital for applications such as point-of care diagnostics and clinical applications. Moreover, they provide faster analysis and lower response times because of the short distance between the sensor and the target and higher surface to volume ratios. Because of their small volume, they need lesser amounts of reagents, resulting in low cost and a compact structure. In addition, miniaturized on-chip biosensors have very low manufacturing costs when fabricated in mass production.

1.2.3 Challenges

The development of new miniaturized biosensors utilizing membrane protein interfaces and microsystem structures faces several challenges in design, integration and fabrication. These challenges must be overcome to fulfill the requirements of specific applications, especially for high density biosensor arrays. High density arrays require routing of hundreds of raw signals off the array chip, introducing bandwidth challenges as well as performance-limiting noise. Similarly, measurement speed has an impact on the performance of the system because the microsystem should be able to record all important data [44]. Moreover, the minimum detectable signal is an important parameter that is affected by

biochemical noise (shot noise of binding/reaction events), interference of background molecules and readout circuit performance [45].

Different applications favor different interrogation techniques and analysis methods, so there is a growing need to design diverse and versatile systems that are capable of performing multiple interrogation techniques to support a range of analysis suitable for many applications. For example, combining optical and electrochemical detection schemes in a single CMOS IC would allow simultaneous optical and electrochemical analysis of on-chip biosensors. This is highly desirable because it would combine the advantages of both these techniques and result in a high throughput system with added functionality, improved accuracy and minimized cost. However, realization of such a microsystem is challenging in terms of electrical design, integration of techniques, fabrication and packaging. Both optical and electrochemical detection system needs to be developed and integrated in an efficient way that permits simultaneous optical and electrochemical detection. To realize a miniaturized and multimode electrochemical detection system, it is desirable to realize the following techniques within the readout IC: cyclic voltammetry (CV), linear sweep voltammetry (LSV), constant potential and normal pulse voltammetry (NPV). These techniques require different input waveforms, so a programmable waveform generator is needed to generate these waveforms. Namely, a triangular, linear ramp, and constant potential generator are needed for the above-mentioned techniques to increase the throughput of the system. Although industry-standard CMOS fabrication processes provide low manufacturing costs, a high level of integration and significant design flexibility, they introduce several important

limitations. For example, another significant challenge in on-chip electrochemical transducers is the lack of a good electrode material in the standard CMOS process. In CMOS ICs, only the top metal layer (aluminum) is exposed to the surface, and aluminum is not as useful with potential electrolytes as gold, platinum, titanium or Ag/AgCl [25, 46]. Thus, post-CMOS fabrication processes are required to protect (insulate) the CMOS top-layer metal and create useful electrodes on the surface of the chip where direct exposure of electrolytes will occur.

For optical detection, CMOS is suitable for visible range photons (320-780nm), although photons in the UV (100nm-350nm) and IR (700nm-300μm) range cannot be effectively detected using CMOS photodiodes because of silicon material characteristics as shown in Figure 1.2 [47]. Proper choice and design of photodiode with efficient readout is needed to increase its responsivity and quantum efficiency for a specific application. Also, to obtain the desirable optical information, filters are required to be incorporated within the optical detection system. For example, in fluorescence detection, only the emitted light from a fluorophore is required to be processed while the excitation light should be blocked using a filter. Typically, post-CMOS processing is carried out to incorporate these filters in the microsystem [48-50], increasing the cost and also increasing the risk of effecting other components and hence functionality of the system. Furthermore, for a combined opto-electrochemical system with on-chip biointerfaces, incorporating filter using post processing is not feasible as it hinders electrochemical detection by separating the electrode from the on-chip readout circuitry. Thus, for optical detection either a filterless approach is required or a new filter design is needed that

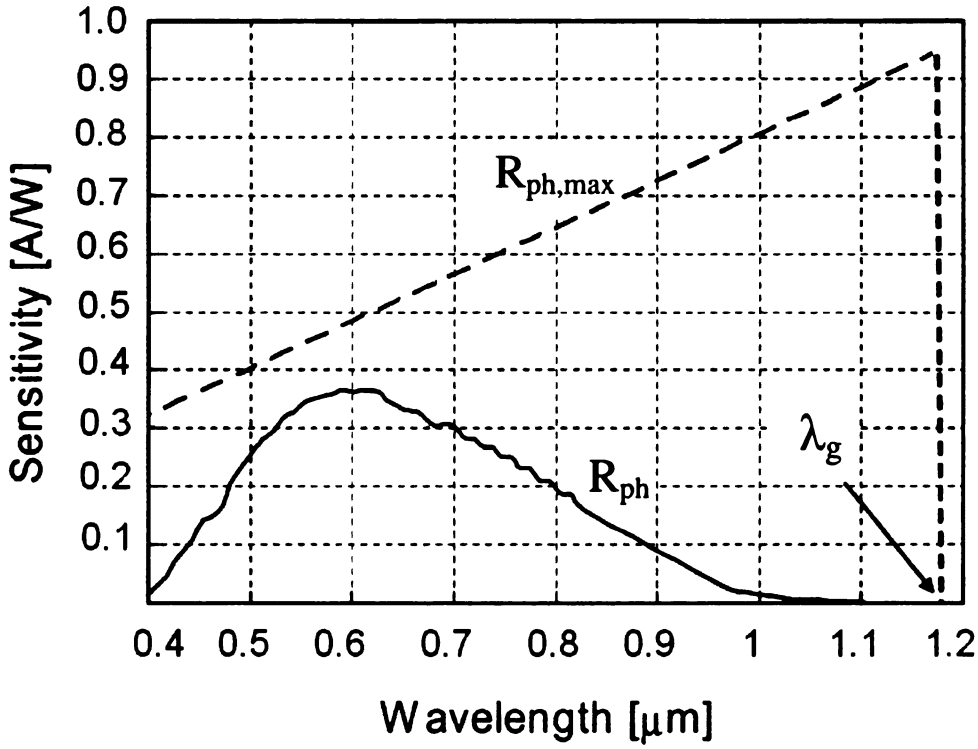

Figure 1.2. Sensitivity of silicon at different wavelengths [47].

can be incorporated in the combined system without the need for post-CMOS processing to allow for simultaneous optical and electrochemical detection.

1.4 Goals

The operation of membrane protein sensors requires the presence of a fluidic environment. Optical detection shows high compatibility with microfluidics and does not require physical interconnection between detector unit and the microfluidic device, resulting in minimal disturbance to reaction system; however, at the same time it suffers from relatively poor detection limits [48]. Electrochemical detection has the advantage of excellent sensitivity with the realization of on-chip electrodes. A combined opto-electrochemical detection system would combine the advantages of both these techniques resulting in an efficient, versatile and high throughput detection system that can be used for a variety of applications.

This research is based on establishing the design of a combined opto-electrochemical detection system for membrane-based protein biosensor array that simultaneously implements both optical and electrochemical detection by first analyzing the challenges to implementing such a system and, secondly, developing a solution for some of the resulting electronics design challenges. A block diagram of the CMOS opto-electrochemical detection system concept is shown in Figure 1.3. The CMOS instrumentation chip assembly is mounted on a *biomembrane array module* daughterboard that is plugged into a *receiver module* motherboard for connection to a standard computer. The receiver module has an open window over the biomembrane array area permitting access to an optical excitation source, a top-side reference electrode and top-side fluid delivery/removal. A data acquisition card (DAQ) within the computer provides programmable control of stimulus, measurement, and fluidic operations.

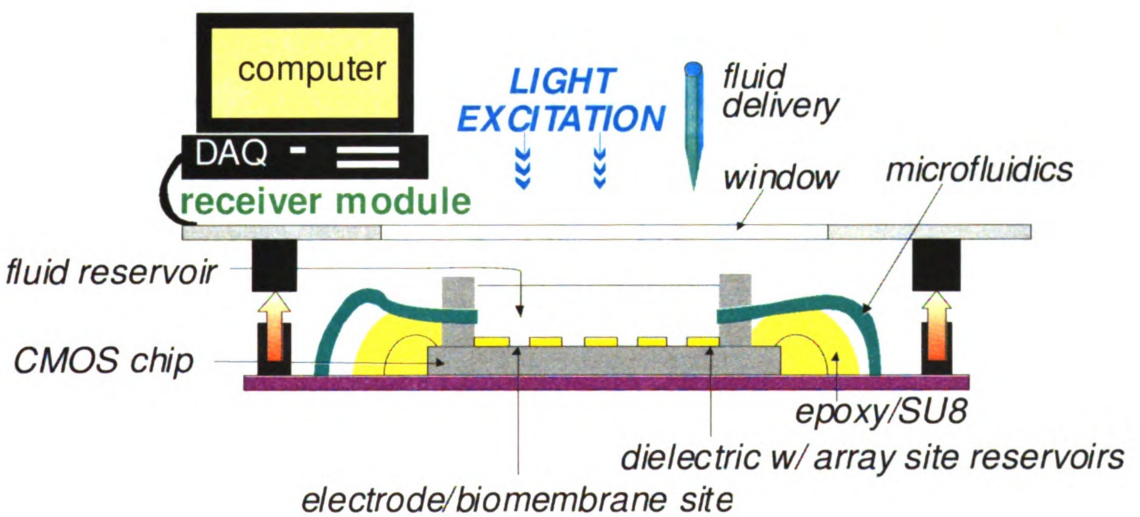

Figure 1.3 Conceptual block diagram of a CMOS opto-electrochemical detection system

To meet the requirements of a combined opto-electrochemical detection system that can be used for a diverse set of biosensors, one goal of this research is to design a multi-mode voltammetry instrumentation system that includes a programmable waveform generator to generate different input waveforms i.e. triangular, linear ramp and constant potential with programmable frequency and amplitude. These waveforms are needed to perform a variety of voltammetry applications including cyclic voltammetry, linear sweep voltammetry, constant potential and pulse voltammetry.

Another goal of this research is the design of a highly efficient optical detection system that meets the requirements of an opto-electrochemical detection system. To avoid the necessity of an optical filter using post-CMOS processing, the final goal of this research is to explore an on-chip filter that relies on a novel technique using the metal layers inherently present in the standard CMOS process. Fabrication of miniaturized on-chip electrodes and development of miniaturized biosensors and bio-interfaces on a CMOS IC for a combined opto-electrochemical detection system are beyond the scope of this research. These challenges are being addressed by other fellow students in the Advanced Micro-Systems and Circuits lab at Michigan State University.

1.4 Thesis Outline

Chapter 2 reviews optical and electrochemical detection methods relevant to the goals of this thesis research. Chapter 3 outlines the issues and challenges regarding the design of a combined monolithic opto-electrochemical detection system along with the background and importance of CMOS opto-electrochemical

detection systems. Chapter 4 discusses the design and VLSI realization of the proposed electrochemical detection system for different voltammetry applications. Chapter 5 describes the proposed system for optical detection using fluorescence and a CMOS interference filter, with an in-depth view of the circuit-level implementation of the proposed technique. Chapter 6 presents and discusses the simulation results and experimental results for several VLSI circuits developed for the proposed fluorescence and electrochemical detection system for membrane protein assays. Chapter 7 provides the summary of the completed research work and gives some suggestions for future work in this area.

Chapter 2
Review of On-chip Biosensor Technologies

2.1 Signaling Mechanisms

Because membrane proteins play a vital role in biological functions and drug discovery, an ability to characterize their activities and incorporate them into sensors is very important. Membrane-protein-based biosensors are used to detect drugs, neurotransmitters, hormones, toxins, and inhibitors such as amiloride [42]. Characterization of membrane proteins is done by using both labeled and label-free detection schemes, each with their own advantages. Label-free detection schemes provide direct detection of analytes without requiring labels, marker compounds added incorporated within a test solution. It generally uses a transducer to measure some physical property or characteristics of a biochemical target, i.e. DNA molecule, protein, virus, or cell. Electrochemical detection is a widely used continuous label-free detection scheme for characterizing membrane proteins. On the other hand, labeled detection methods require modifying the target molecules with labeling compounds. Optical detection methods can use both labeled and label-free detection schemes for characterizing membrane proteins, e.g. chemiluminescence and fluorescence. Fluorescence detection is one of the most widely used labeled optical detection schemes to characterize the membrane proteins.

2.1.1 Luminescence

Luminescence is defined as a process by which light is produced my means other than heating or incandescence. This light can be emitted at normal or lower temperatures and is also named as "cold light". This phenomenon occurs due to a

change in the energy level of an atom, an ion or a molecule. For example, by absorbing energy from an excitation source, an electron of an atom is driven from its lower energy level or ground state to a higher energy level, as shown in Figure 2.1(a). This higher energy state, which is unstable, is called an excited state, and whenever the electron comes back to its lower energy level then a photon of light may be emitted. The photon energy corresponds to the difference between energy levels, shown in Figure 2.1(b). Usually the emitted light has less energy as compared to the energy of excitation light. Based on the source of excitation light, there are several different types of luminescence: fluorescence, chemiluminescence, optically simulated luminescence, cathodoluminescence, radio luminescence phosphorescence, electroluminescence, triboluminescence and thermo luminescence.

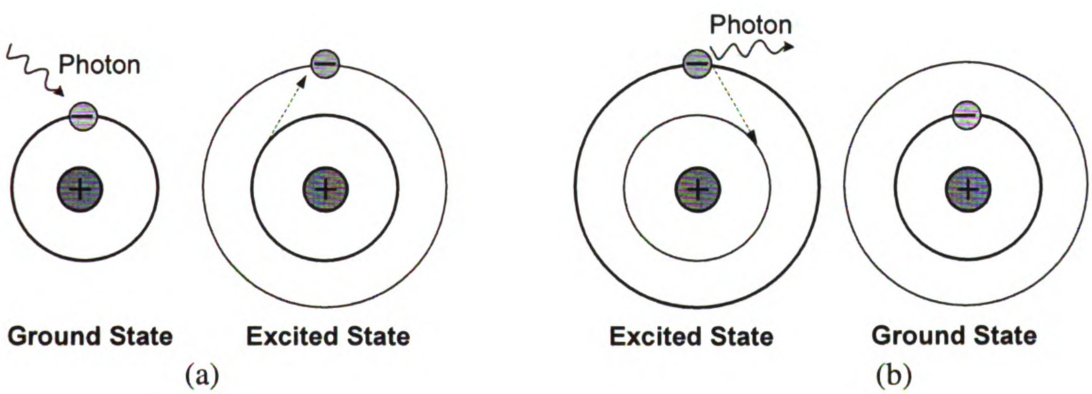

Figure 2.1. Absorption and emission of energy due to change in energy level.

2.1.2 Fluorescence

According to the Columbia Encyclopedia; **fluorescence** is defined as the "luminescence in which light of a visible color is emitted from a fluorophore under stimulation or excitation by light or other forms of electromagnetic radiation or by certain other means". This emitted light or radiation persists as long as the

stimulating light continues, and it has a longer wavelength as compared to the excitation light. This process of changing energy states or levels is shown in Figure 2.2. Some of the important characteristics of fluorescence are as follows.

(a) Stokes Fluorescence: Fluorescence can be defined as the re-emission of longer wavelength photons by a molecule that has absorbed photons of shorter wavelengths. In other words, emitted light has less energy than the excitation light or absorption light because of loss of vibrational energy in the excited state [49]. Thus, the fluorescence occurs at longer wavelengths i.e. $hv_F < hv_A$ as shown in Figure 2.3. This change is wavelength is typically referred to as the Stokes Shift.

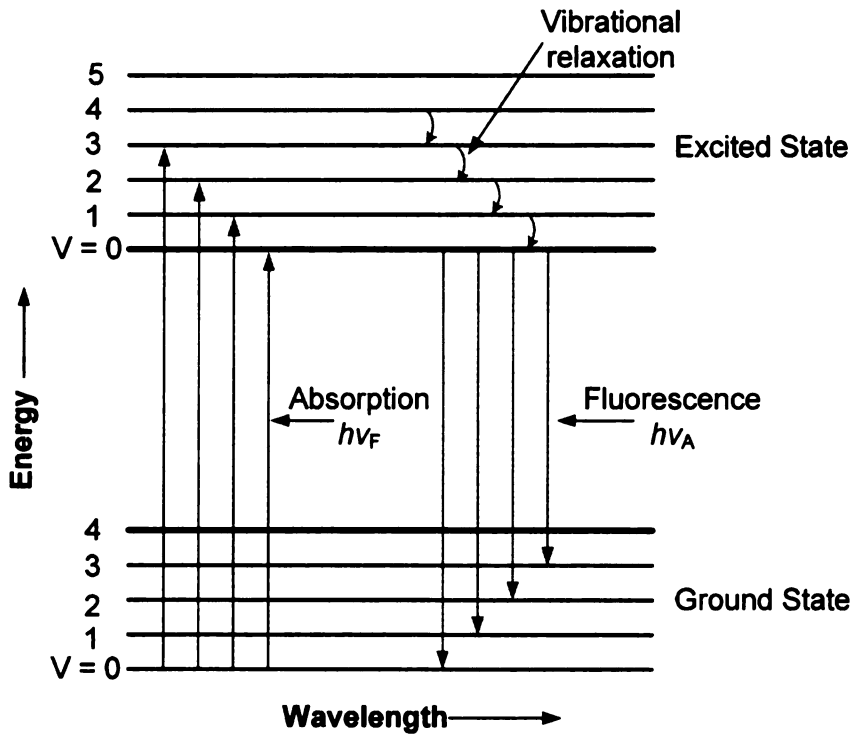

Figure 2.2. Fluorescence occurrence due to change in states.

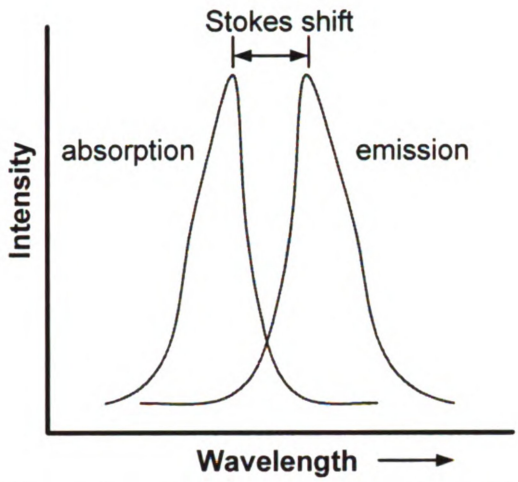

Figure 2.3. Absorption and emission phenomena in fluorescence.

(b) Lifetime: One of the important characteristics of fluorescence is its lifetime. The lifetime of the excited state is determined by the average time the molecule spends in the excited state until it returns back to the ground state or lowest energy level. Fluorescence is considered to be a very short lifetime phenomena, on the orders of nanoseconds. This lifetime can change to some extent with changes in the fluorophore environment.

(c) Quantum Yield: The fluorescence quantum yield, Φ, is the ratio between the number of fluorescence photons emitted and the number of photons absorbed by a detector.

$$\Phi = \frac{\text{No of photons emitted}}{\text{No of photons absorbed}} \tag{2.1}$$

2.1.3 Electrochemical detection

Because of its high sensitivity and excellent selectivity, **electrochemical detection** is used in many biomedical and environmental applications. Output depends on the nature of the current flow, i.e. oxidation or reduction current due to the input voltage applied and properties of the electrode. The electrochemical

detector typically contains three electrodes: a working electrode where the chemical reaction takes place, counter electrode that supplies current, and reference electrode which acts as zero potential for the working electrode. Because of its highly stable characteristics, Ag/AgCl is the most widely used reference electrode. The counter (or auxiliary) electrode is usually made of an inert material such as noble metal or graphite.

A potentiostat is the basic electronic element in electrochemical detection schemes. It is used as a biasing circuit and provides an electronic interface to the detector. It controls the potential between the working and reference electrodes while a current readout circuit measures the current between the working and counter electrodes. Different approaches for both single-ended and differential CMOS potentiostats with a variety of readout circuits have been reported [50-60]. Two of the most widely used electrochemical detection techniques using these potentiostats are voltametry and impedance spectroscopy.

2.1.3.1 Voltammetry

Voltammetry is a widely used electrochemical technique in which different types of voltage waveforms are applied at the working electrode and response current is measured. Based on the input waveform, the different voltammetric techniques used include cyclic voltametry (CV), linear sweep voltametry (LSV), constant potential or DC voltametry and pulse voltametry. Out of these techniques, CV is the most effective and widely used technique to study the formal redox processes for many applications. In CV, a triangular waveform with a specific rate and amplitude, referred to as scan rate and scan range, respectively, is applied at the

WE (w.r.t the RE) and the response current is measured between WE and CE, as shown in Figure 2.4. In linear sweep voltametry, a linear ramp is applied at the WE, and in the case of constant potential or dc voltametry, a constant potential is applied and response current is measured.

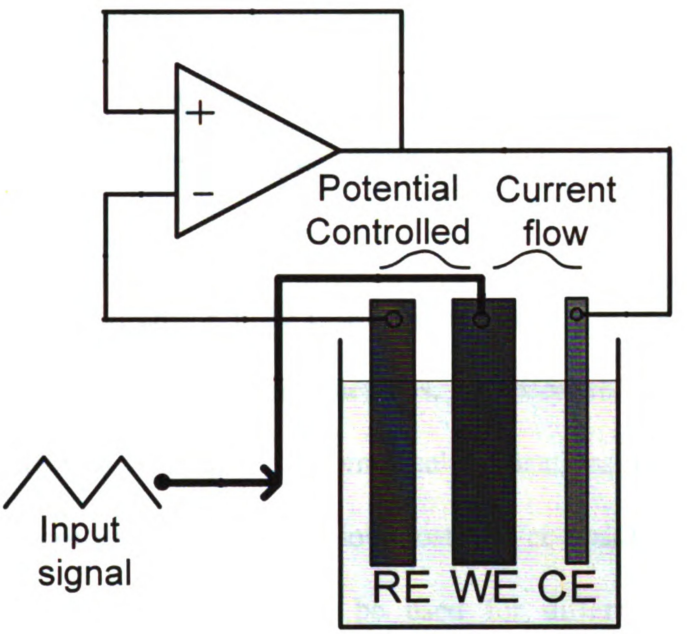

Figure 2.4. 3-electrode electrochemical system using cyclic voltammetry.

2.1.3.2 Impedance Spectroscopy

Impedance spectroscopy (IS) is another widely used non-destructive electrochemical detection technique in which the relationship between the stimulus potential, response current, and frequency of stimulus is measured to characterize the impedance. In IS, an AC potential is applied to an electrochemical cell and the response current containing both real and imaginary components is measured for each frequency of input stimulus. Sometimes these measurements are made in the time domain and then fourier transformed into the frequency domain.

Electrochemical impedance spectroscopy (EIS) involves measurement and analysis of materials in which ionic conduction strongly predominates. This technique can be used to analyze different processes including electronic/ionic conduction in the electrode and electrolytes, interfacial charging either at the surface film or the double-layer, charge transfer processes and the mass transfer effects, if any [61]. As these parameters have different responses at different frequencies, their features will also show at different frequencies of the impedance spectrum.

2.2 Approaches for On-chip Fluorescence Detection

Of the reported optical detection methods, fluorescence has emerged as the most attractive detection technique for biomedical applications due to its excellent sensitivity and specificity as well as its low cost and compatibility with CMOS technology. Fluorescence detection can be used for different applications in biophysics, biochemistry and medical diagnostics [62-66] . The basic components of an on-chip instrumentation system for fluorescence detection include an excitation source as a source of light of a specific wavelength, a photo detector to detect light, and a transducer to convert the optical response signal into voltage so it can be interfaced with a readout circuit to measure the intensity that correlates to concentration. In a biosensor with optical detection, photodiodes are typically used to transform biological information into electrical signals.

Different approaches have been reported for fluorescence detection and imaging including various types of fluorophores with different configurations of photodiodes. The fluorophores reported for fluorescence detection are derivatives of

Rhodamine, Fluoroscein, Coumarin, Europium and Cyanine [67-71], as best suits each application. The two primary types of sensors for imaging applications are charged coupled devices (CCD) and complementary metal oxide semiconductors (CMOS) imagers. Both CCD and CMOS image sensors can be manufactured in silicon technology foundries using standard materials and equipment. Commonly, fluorescence detection utilizes CCD detectors and external signal processing circuitry. However, because of fabrication differences, CCD detectors cannot be integrated on the same chip as normal integrated circuits (IC) used for signal processing. In contrast, CMOS-based optical detectors can detect fluorescent emission within the same IC as signal processing circuitry [72]. Additional advantages of using CMOS-based detectors include ease of design, low cost, low power consumption and small-size detection circuits [73].

2.2.1 Fluorescence detection using CCD image sensors

Because of better image quality and better performance in terms of dynamic range and noise, a variety of on-chip and off-chip fluorescent detection systems have been developed using CCD image sensors [74-76]. These detection systems have been used for different applications including pathogen detection and myoglobin detection by immobilizing antibodies on the surface of immunosensors.

2.2.2 Fluorescence detection using CMOS image sensors

Fluorescence detection using **CMOS image sensors** have widely been reported using different types of photodiodes and readout topologies tailored to specific applications. The main advantages of CMOS photodiodes over CCDs include low cost, high speed, and high responsivity. CMOS image sensors also offer

superior integration capabilities with lower power consumption at the expense of image quality.

For fluorescence measurements using CMOS imagers, different photodiodes are available to sense light intensity which is measured using on-chip microelectronic circuits. Light intensities as low as ~10^5 photons/cm^2 have been reported using advanced circuit topologies [77-79]. The different photodiodes that have been used include p-n, PIN and avalanche photodiodes [80-82]. Similarly different readout topologies including differential photodiode (PD) [83], pseudo-differential active pixel sensor(APS), 3T APS and 4T APS [47, 78] have also been reported to measure low light intensities. Although very large pixel array using CMOS photodiodes have been reported [84-86], fluorescence applications often emphasize quantification of light rather than pixel density. Thus, moderate sized arrays that permit greater area per pixel can be chosen to loosening design constraints.

2.2.3 Optical filters

Optical filters are commonly used to selectively block excitation frequencies while transmitting the fluorescent emission signal. Different materials and processing steps have been reported to incorporate optical filters into fluorescence detection systems. In [87] a fluorescence detection microsystem has been proposed by integrating a Cadmium sulfide(CdS) thin-film filter, an (In,Ga)N thin-film blue LED and a disposable PDMS microfluidic device onto a Si PIN photodetector substrate. The process includes deposition of a 1-3μm thin-film CDS filter on a stacked ITO/SiO_2 layer using pulsed layer deposition (PLD). SiO_2 layer with a

thickness of 1500A° was deposited by PECVD on silicon photodiode substrate, while ITO film with a thickness of 2000A° was deposited using sputtering mechanism. Deposable microchannels were fabricated on a PDMS mold that was prepared using deep reactive ion etching (DRIE). Although this microsystem was able to detect fluorescence and also CdS film filtered the emitted signal but it has many limitations in terms of performance as an appreciable amount of light is reflected from the backside of microfluidic device. Also for better performance it needs addition of antireflection coating to the CdS film to suppress the reflection of emission signal. Moreover larger PIN photodetector area is required to increase the collection of emitted signal. These factors severely affect the performance and cost of this detection system as it needs extra processing steps to achieve good performance. Similarly in [88] a monolithic capillary electrophoresis system with an integrated on-chip fluorescence detection system has been proposed which includes a Si photodiode combined with an on-chip multilayer interference filter to prevent excitation light from hindering the fluorescence detection. This 3μm filter consists of 20 alternating layers of SiO_2 and TiO_2 at nearly quarter wavelength thicknesses. Although this technique integrates photodiode with the filter on a single substrate, it requires extra processing steps that add cost and complexity and are not available through a standard CMOS foundry. In [89] a fluorescence detection system has been proposed in which a cross polarization scheme is being used to separate excitation light form emission spectrum. A bi-layer organic photodiode (OPD) consisting of duplicate layers of CuPC and C_{60} with ITO anode and aluminum cathode increasing the photodiode quantum efficiency. Similarly a

monolithically-integrated sensor on a microfluidic platform is presented integrating a vertical-cavity surface-emitting laser (VCSEL), PIN photodetectors and optical emission filters on a GaAs substrate and coupled to a glass microfluidic channel using a discrete micro-lens which is used to both focus the laser beam into the microfluidic channel and adjust the emitted fluorescence into the photodetector [90].

The concept of diffraction grating has been used for optical modulation and filtering by introducing grooves on the top layer to diffract light at different angles based on their wavelength and angle of incidence. In [91] a monolithic optical phase shift detector on silicon has been reported that generates a current based on relative phase difference between two incident beams. It consists of a single diffraction grating layer etched at the surface of p-n photodiode. The proposed system need extra elements e.g. a mixing element to project the two incident beams into one or more common directions where they interfere, and also requires proper placement of photodetectors at the right place to pick-up the interference products. In [92] a micromachined optical modulator with electrostatic actuation has been reported, fabricated by the conventional CMOS process. The optical modulator is operated by the interaction of single-layered fixed stationary gratings and moveable sliding gratings, where the period of gratings is determined by the slide of the moveable part which allows different diffraction patterns of reflected light. These diffraction patterns differ according to the wavelength, incident angle, depth and period of grating. This fabricated optical modulator still needs extra post-processing to obtain a high-aspect-ratio microstructure.

For optical filtering another diffraction grating approach is reported in [93] where analytical models were designed by using available metal layers in the standard CMOS process. These metal layers are patterned in the complex structure of CMOS photodiodes and act as a color filter to select a desirable wavelength. The width of these metal layers and separation between them are manipulated to act as a diffraction grating. For selecting a proper wavelength the pattern of metal layers needs to be optimized. Although this approach is used for color filtering, there is no discussion about blocking scheme of undesirable light and also about the number of metal layers i.e. whether single-layered or multilayered diffraction grating is used. Also there are no actual measurement results from the chip that validate the analytical model.

2.2.4 Filterless techniques

Although filters enable fluorescence detection and are compatible with many biomedical applications, standard filters add bulk and complexity that are incompatible with integration into a microsystem platform. To address this problem, techniques have been developed to bypass the need for optical filters.

Detection systems based on **time-resolved fluorescence spectroscopy** have been proposed which do not need optical filters. In [94] real-time photodetection has been implemented by extracting the transient fluorescence decay response. Laser excitation was controlled by a fast clock from the chip to measure the exponential decay of a fluorophore. Photocurrent response from the photodiode was integrated repeatedly at different start times, and results of multiple measurements were averaged to achieve high signal-to-noise performance. Similarly to improve

detection sensitivity, multiple measurements at the same start time were taken and averaged. The output transient current, which is directly proportional to fluorescence intensity, was generated by numerical differentiation. An 8x4 pixel array was divided into four banks of eight pixels with a current-mode ΣΔ analog-to-digital converter (ADC) sampling the output from a current-mode sample-and-hold circuit (SH) within each bank. Signal current from each pixel, which consists of an n-well/p-sub photodiode and a front end readout circuit, are time-multiplexed onto a single current-mode SH composed of a differential transconductor with two feedback storage capacitors. This CMOS sensor array build in a 0.5μm process was able to measure fluorescence with a sensitivity of 10^8 photons/cm^2, a dynamic range of 74dB, and sub-nanosecond timing resolution. In [95] a relatively large 64x64 sensor array was built in a 0.18μm process utilizing the same technique with a differential photodiode and per-column ADC, reporting a sensitivity of 8.8×10^6 photons/cm^2 and sub-picoseconds timing resolution.

A similar technique was utilized for fluorescence detection by using different readout topologies and photodiodes. In [96] a two-chip vertically integrated CMOS microsystem consisting of 8x8 AlInGaN blue micro-LED array for the excitation pulse, and a 16x4 array of single-avalanche photodiodes (SPAD) to detect fluorescence emission was proposed for time-resolved fluorescence analysis. This microsystem was fabricated in a 0.35μm high-voltage CMOS process and included in-pixel time-gated photon counting circuitry. Detection sensitivity down to concentrations of 10nM was demonstrated. Although this system provides good performance, the SPADs require high voltages ~20V that are not suitable for

low-power and portable microsystems. The same is true for [82, 97, 98] where CMOS SPADs were used with different readout topologies for photon counting; all of these microsystem require high voltage for the SPADs to detect photons.

2.2.5 Analysis and Discussion

Although integration of filter layers using post-CMOS processing has better performance and blocks the excitation light efficiently, it also adds to the cost of detection system and needs proper isolation so that it does not affect the other components of the system. Also, this technique is not suitable for a combined opto-electrochemical system where no filter layer can be inserted between photodiode and the fluorophore because of fluidic environment.

Single-layered diffraction gratings compatible with CMOS process are useful for optical modulation of light. But for multi-color imaging that requires filtering, multi-layered diffraction grating is required to select the specific wavelength of light. Moreover selectivity of the filter can be increased to a large extent by using extra metal layers patterned in an optimized manner that can be used for 1) extra blocking of undesirable light 2) increasing the selectivity by blocking the light that is passed thorough the edges of top metal layers.

Time-resolved fluorescence spectroscopy has the advantage of fluorescence detection without using optical filters; it reduces the cost and does not require post-CMOS fabrication process. However, this technique also suffers from limitations in the design. As fluorescent light has a very short life time (nsec–psec), time-resolved fluorescence spectroscopy need a very high clock rate to separate the excitation light from emission light. Also this clock needs to be strictly accurate with

minimum skew and jitter. On-chip high frequency clock generation leads to extra design complexity with adverse effects on noise, CMOS area and power consumption, while off-chip clock generation adds to system cost and bulkiness. Moreover, because of some overlap of excitation and emission light, there is some loss of information when the clock is used to turn-on and turn-off the arrival of input photons to the photodiode. Thus, there is a need for an alternative efficient fluorescence detection system that is highly sensitive, accurate and portable.

In time-resolved fluorescence, the response time of the photodiode also has a critical role. With the high speed clock that alternately turns on/off the photodiode, the photodiode response should be fast enough to generate electron-hole pairs (EHP) within that time. Larger diode area increases the sensitivity and fill factor, but at the same time increases diode capacitance and reduces response time due to large RC time constant. Thus, time-resolved fluorescence may not be a suitable technique when large diode areas are required.

2.3 Approaches for on-chip Electrochemical detection

2.3.1 Voltammetry

Different on-chip CMOS electrochemical detection systems have been proposed and used for voltametry applications. In [99] an electrochemical array microsystem was proposed that uses a high performance CMOS potentiostat and amperometric readout circuit that supports cyclic voltammetry assay techniques. Post-CMOS fabrication was done to develop an electrode array on the readout chip. Similarly, [100] reports the development of a sensor using diamond-coated, micro-needle electrodes and a readout chip designed in 0.5μm CMOS for neurochemical

monitoring in the nervous system using fast-scan voltammetry. Moreover, interdigitated gold electrodes have been fabricated with a CMOS circuit for electrochemical detection of dopamine, and CV was performed using these microelectrodes to identify the respective oxidation and reduction potentials for dopamine in a phosphate buffer solution [101]. Similarly a differential potentiostat circuit with differential recording electrodes implemented in 0.35μm CMOS was reported for fast scan cyclic voltammetry (FSCV) with improvement in the dynamic range [102].

2.3.2 Impedance Spectroscopy

In [103] a compact, high sensitivity impedance to digital converter (IDC) was reported with sensors array for impedance spectroscopy. Similarly, in [104] a fully integrated electrochemical impedance spectroscopy (EIS) biosensor array was presented, enabling flexible, parallel and electronic bio-molecular detection. Measurement results of label-free detection for DNA, BSA and protein G in different frequency ranges was presented. Moreover, in [105] a 4.4mm x 4.4mm chip consisting of 4 x 4 electrode array with a fully integrated interface circuit was implemented for stimulation and recording of the activity from electrogenic cells. The electrode-electrolyte interface was characterized using EIS to model the interface with an equivalent circuit.

2.3.3 Analysis and Discussion

Although efficient electrochemical detection systems have been reported, a versatile and multimode electrochemical detection system that can be utilized for a variety of applications is not currently available. There remains a need for a

versatile detection system that is capable of multiple voltammetry techniques. These techniques require different input waveforms to be applied to the potentiostat, so a programmable waveform generator capable of controlling the frequency (scan rate) and amplitude (scan range) is an essential component for an efficient and multimode voltammetry instrumentation system. Moreover, highly sensitive and efficient CMOS readout circuit needs to be implemented that are capable of measuring currents within the fA range.

2.4 Integration of optical and electrochemical detection

Membrane proteins play a vital role in cellular functions and there is a pressing need to understand the structure and functions of these membrane proteins. For better understanding and more accurate analysis of membrane proteins different detection techniques could be combined that can simultaneously measure the molecular mechanism from different aspects. Optical and electrochemical detection techniques show great promises to be combined on a monolithic chip resulting in multiple analysis of membrane proteins at the same time from different aspects with an improvement in the detection accuracy and analysis.

In order to realize a versatile miniaturized opto-electrochemical instrumentation system, all of the challenges described above need to be addressed. This task requires a multidisciplinary approach coving biointerface development, microfabrication, and CMOS circuit design. The following chapters describe efforts to address the most critical challenges that can be solved through innovative design of CMOS circuitry. These efforts form the basis of this MS thesis research and include 1) a thorough analysis of the challenges for combining optical and

electrochemical detection in one system, 2) the design of a multi-mode voltammetry circuit enabling different voltammetric techniques and 3) the design of an optical detection circuit with an integrated on-chip optical filter that does not require post-CMOS processing and also does not hinder electrochemical detection.

Chapter 3
Integration of Optical and Electrochemical detection

3.1 Motivation

Combining optical and electrochemical detection in a single chip permits simultaneous determination of multiple biomembrane processes and is therefore highly valuable, e.g., to characterize multi-protein membrane complexes that are regulated by a wide range of interacting partners. This combination results an improvement in the ability to measure biomembrane phenomena and helps to better understand these phenomena with significant impact, for example, on field of materials science, where there is a need to develop functional nanomaterials that exhibit a desirable safety profile. Multiple analyses can be carried out simultaneously on a particular membrane protein and interaction between different molecular phenomena across a membrane-protein or an array of different membrane proteins can be measured. This results in a versatile, efficient, high throughput instrumentation system with the advantages of both optical and electrochemical detection techniques. Also, these two techniques can be compared to verify the output of each other, increasing the accuracy and reliability of the overall system.

3.2 Background

Some detection systems have been reported for opto-electrochemical detection using off-chip imagers for optical detection and off-chip electrodes for electrochemical detection[106, 107]. However, these systems are bulky, expensive and less efficient than an on-CMOS microsystem realization. Despite their

advantages, CMOS opto-electrochemical detection systems on a monolithic chip introduce several challenging obstacles that are only beginning to be addressed by research.

In [108] a label-free optical approach was proposed to quantitatively measure "localized electrochemistry" on a 10μm spot on a single planar electrode using a single-channel potentiostat by monitoring the modulation of charge at the electrode interfacial layer (EIL) during the redox process. Although the proposed optical and electrochemical setup is not a CMOS-based approach, it highlights the opportunity to develop a CMOS-based instrumentation system for opto-electrochemical detection system.

An instrumentation chip that combines optical and electrochemical detection and implemented in 0.35µm CMOS process has been reported [109]. The sensor uses a combined 128 x 128 optical and 8 x 8 electrochemical pixel array with readout circuitry. The optical detection circuit uses off-chip color filter resist layer to separate fluorescence light form excitation light which require post-CMOS processing resulting in an increase the cost of the system and complexity. Also, these off-chip filters severely limit the functionality of the proposed system within a microsystem platform. Moreover, for electrochemical detection the readout circuit suffers from low sensitivity (nA) which needs to be improved to the pA-fA range for an effective system. Moreover, the CV profile obtained from the on-chip electrodes is unbalanced and unstable, which has a deteriorating effect on the performance of this microsystem. In addition, the proposed system requires an external signal generator to perform cyclic and differential pulse voltammetry,

which limits its use in portable applications. Finally, no performance results have been shown for differential pulse voltammetry. For an autonomous and efficient multi-mode voltammetry system, a waveform generator needs to be integrated on the same chip that can be programmed to generate waveforms for different types of voltammetry e.g. CV, LSV, constant potential and pulse voltammetry. All of these limitations should be taken care of for an efficient opto-electrochemical detection microsystem.

3.3 Challenges for opto-electrochemical detection

The integration of optical and electrochemical detection for simultaneous operation on a monolithic chip is tremendously beneficial for measuring multiple sensor interface activities. Such a system would be highly valuable for many applications, but its implementation is challenging. Apart from the requirements and challenges discussed in Chapter 1 for electrochemical and optical sensors individually (high selectivity, sensitivity, accuracy, portability and high throughput), a combined instrumentation system introduces critical additional requirements and challenges. These include the design of: 1) a CMOS-compatible sensor interface suitable for both optical and electrochemical detection, 2) a highly selective optical filter that blocks the excitation light source from the optical detector without hindering electrochemical detection, 3) a multi-mode electrochemical detection system with added functionality including a waveform generator for different voltammetry techniques, 4) a highly sensitive and efficient readout circuits to measure very low currents, 5) a microsystem scheme that

minimizes interference between electrochemical and optical sensors, and 6) proper system integration and packaging.

To maximize the advantages of combined optical and electrochemical detection, these measurements are required to be taken at the same time. One of the main considerations for combining these techniques is their operating frequency. Electrochemical sensing for bilayer membranes is carried out at very low frequencies (mHz) while fluorescence detection is carried out at relatively high frequencies because of the very short lifetimes (decay rate ~nsec-psec) of emitted light. For fluorescence detection, the photodiode is exposed to light for a very short time, and larger time may cause saturation of the photodiode. Thus, the photodiode needs to be turned on/off relatively with a fast pace. In contrast, for electrochemical detection, sensing electrodes are exposed for a much longer time to the electrolyte. So both these sensing mechanisms are required to be carried out independently and at different rates with no impact on each other.

Optical and electrochemical detection techniques require different stimulus signals with different response times and different output ranges, and they are affected by different noise sources. Thus, the readout circuits for both electrochemical and optical sensors will have different architectures and different requirements. For example, simple *detection* of fluorescence places more significance on the minimum detectable signal (MDS) while *quantification* of fluorescent light has more significance on SNR and dynamic range (DR). On the other hand, for electrochemical detection, DR requirements are less significant while MDS or sensitivity requirements are high [110]. These requirements and

parameters dictate the design of readout circuits for these techniques. Also for simultaneous measurements, performance of the instrumentation system might be affected by the interference between both readout circuits. Noise from both readout circuits need to be isolated and minimized so that it does not affect the performance of the adjacent circuit.

Optical detection circuits need filters to get the desired information. For example, for fluorescence detection, filters are incorporated in the design to block the excitation light while emission light at a different wavelength is allowed to pass through it. Typically, these filters are built between the photodiode and the fluorophore using post-CMOS fabrication. However, for a combined on-chip opto-electrochemical system, these techniques cannot be used because they would isolate the on-chip electrode from the readout circuit making electrochemical detection ineffective. Thus, to realize a combined opto-electrochemical system, either a filter-less approach is required for optical detection or a filter is required that does not provide any hindrance to electrochemical detection.

For both measurement techniques, the geometry (physical structure) of the system has critical effect on performance and functionality. The working electrode for electrochemical detection can be placed on the top of the photodiode, but in that case it should be transparent so that emitted light can pass through it and get absorbed by the photodiode. Because of the relatively large size of the working electrode (~0.1mm^2), this topology would relieve some constraints for optical detection by permitting a photodiode with large area to receive more photons and increase dynamic range. Another approach may be to place both sensors (electrode

and photodiode) side by side with the membrane protein interface on top. This would not require transparent electrodes because there is no hindrance in the path of light, but at the same time it would decreases the fill factor of the pixel as the electrode would cover significant area beside the photodiode. Also, because light travels in all directions, this approach would result in loss of emitted light due to the area covered by electrochemical electrode. Moreover response from adjacent pixels would need to be properly isolated from each other to increase the selectivity and accuracy of the instrumentation system.

The post-CMOS processing required to develop electrochemical electrodes on the chip's surface needs to be highly accurate and selective so that it does not affect the photodiode array on the CMOS IC. Also proper isolation is required not only between electrodes for electrochemical detection but also between photodiodes and electrodes, to minimize the effect of adjacent sensors on the measurement that may impact on accuracy of the system.

Packaging is also an important issue to be considered for the combined opto-electrochemical instrumentation system. Optical detection needs to be carried out with minimum background light to increase the minimum detection limits. Efficient and accurate fluid delivery is also required for a membrane protein biosensor system. Both optical and electrochemical readout circuits need to be protected from the adverse effects of incoming light and fluid interfaces that could adversely affect the performance of the microsystem.

Chapter 4

On-Chip Instrumentation System for Electrochemical Detection

This chapter describes a versatile and multimode CMOS instrumentation system specifically designed for electrochemical detection using multiple voltametry techniques including cyclic voltametry (CV), linear sweep voltammetry (LSV), constant potential voltammetry and normal pulse voltametry (NPV).

4.1 Chip Architecture

The primary targeted application for the on-chip electrochemical detection system is the characterization of thin-film biomaterials, such as redox enzymes, membrane proteins and DNA receptors. These applications utilize very low electrochemical (EC) potential scan rates, in the range of mV/sec, and moderate scan range, below 2V. The three main blocks of a voltammetry-based electrochemical instrumentation system are the voltage waveform generator, the potentiostat and the amperometric readout circuit. For a complete electrochemical detection system, all of these components need to be integrated monolithically on a CMOS chip. An autonomous and versatile CMOS chip would contain all of the necessary instrumentation electronics and a communication interface that permits user control of measurement operations and reporting of measurement results. The chip-scale miniaturization and integration of electrochemical sensors and their instrumentation electronics has many advantages, most significantly extending the limits of detection by improving the signal to noise ratio. The proposed instrumentation chip was designed in a 3M, 2P 0.5μm CMOS process with a 3.3V supply voltage. As shown in Figure 4.1, it includes all three main components of an

electrochemical detection system, namely a digitally programmable signal generator to produce a variety of stimulus signals for different voltammetry measurements, a 2x2 array (4-channel) of single-ended potentiostat for electrode biasing, and an amperometric readout circuit to measure response currents resulting from the stimulus voltage. The chip has the capability to integrate electrodes and sensors directly on the die surface using post-CMOS processing. On-chip measurements permit improvements in sensitivity and immunity from environmental interference by minimizing the length of electrical connections between electrodes and instrumentation circuit and eliminating external wiring.

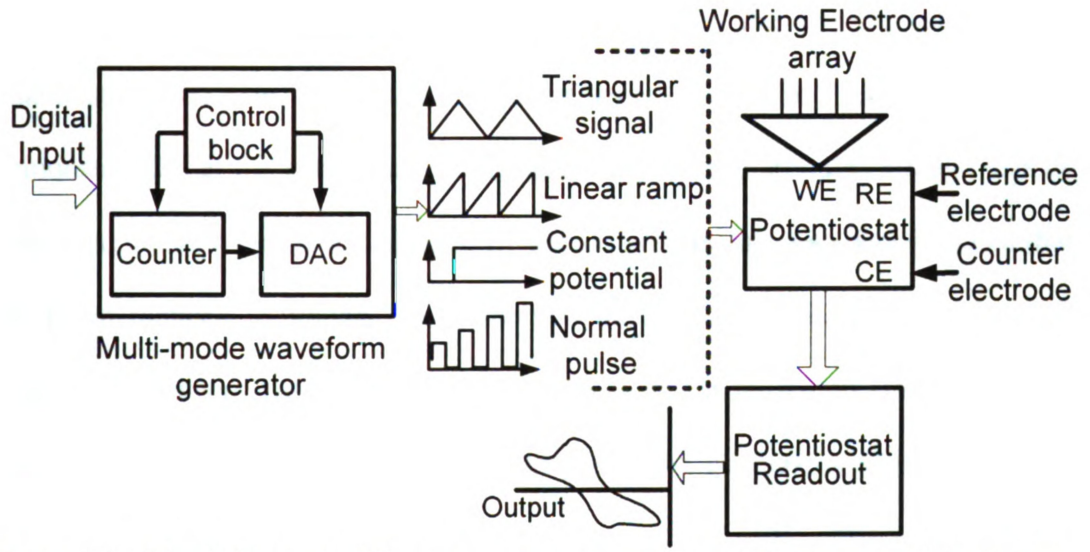

Figure 4.1. Block diagram of the autonomous amperometric instrumentation system.

4.2 Programmable Waveform Generator

A waveform generator is an important component of an autonomous electrochemical instrumentation system that requires different input waveforms for different voltammetric techniques. To fulfill the requirements of the proposed electrochemical instrumentation system, a multi-mode waveform generator is

desired to produce signals of various shapes for different types of voltammetry, amplitudes (scan range) and frequencies (scan rates). Programmable analog circuits could be constructed to generate continuous waveforms, but different analog circuits would be needed for each desired signal shape (triangle, linear ramp, pulse etc.) with an undesirable impact on power and chip size. To avoid the adverse impact of multiple analog waveform generators, a digital solution was explored.

A DAC with a digital controller could implement all shapes, but the output would be quantized and the complexity of the controller could be significant for the desired set of signal shapes. This issue was carefully considered and a variety of designs were explored. A thorough examination of the impacts of stimulus quantization on electrochemical measurements was also performed. Tests demonstrated that the steps (abrupt changes) in quantized stimulus voltage signals generated noise in the output current. However, experiments also demonstrated that the noise reduced as voltage step size was decreased. Through electrochemical experiments, it was determined that, for a 2V scan range, a step size of 8mV or lower produced optimal output results comparable to continuous stimulus signals. This 8mV step size can be realized by using an 8-bit DAC. Although a higher number of bits, i.e. 12, 14, could be used, that would also increase the complexity, power and area of the chip, which is undesirable for electrode arrays on chip. It was also determined that, with careful design, a very efficient digitally controlled waveform generator could be realized with low power and chip area. Therefore, a DAC-based multi-mode waveform generator was developed.

The digitally programmable waveform generator is shown in Figure 4.2. It is composed of a digital control block, a 10-bit comparator, a 10-bit bidirectional counter, and a 10-bit DAC.

4.2.1 Control Block

The control block was designed to generate non-overlapping clock signals and control signals to: 1) reset the waveform generator, 2) control the counting direction of the bidirectional counter using a comparator, and 3) select from multiple waveform modes to enable a specific voltammetry technique. A single pin was used to serially shift the 22-bit configuration input data to the control block as shown in Figure 4.3. Based on this input, the MUX and comparator select the desired signal frequency (Clock), amplitude maximum (S_high), and amplitude minimum (S_low). This on-chip control block also includes a clock divider that provides fine tuning of the scan rate; the output clock can be selected from CLK, CLK/2, CLK/4, or CLK/8, where CLK is the external input master clock.

4.2.2 Bidirectional Counter

For cyclic voltammetry (CV), the input potential is scanned in both positive and negative slopes to stimulate reduction-oxidation (redox) reactions. A bidirectional counter is needed to perform this function. Based on the comparator's output, a 10-bit counter that counts in either direction is needed to produce the required waveform. To meet this need, the counter shown in Figure 4.4 was designed based on a reported counter

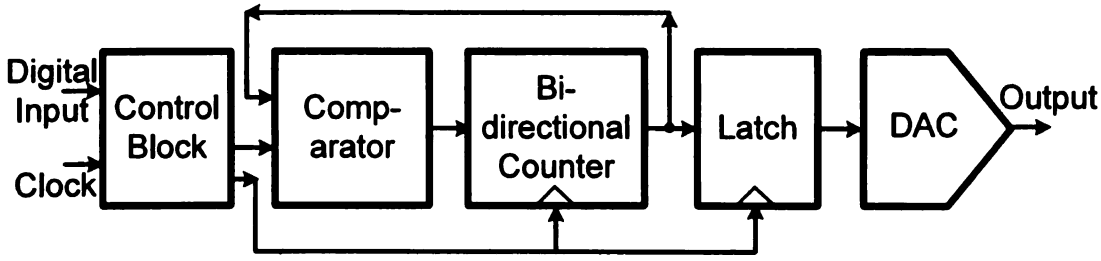

Figure 4.2. Block diagram of the multi-mode voltage waveform generator.

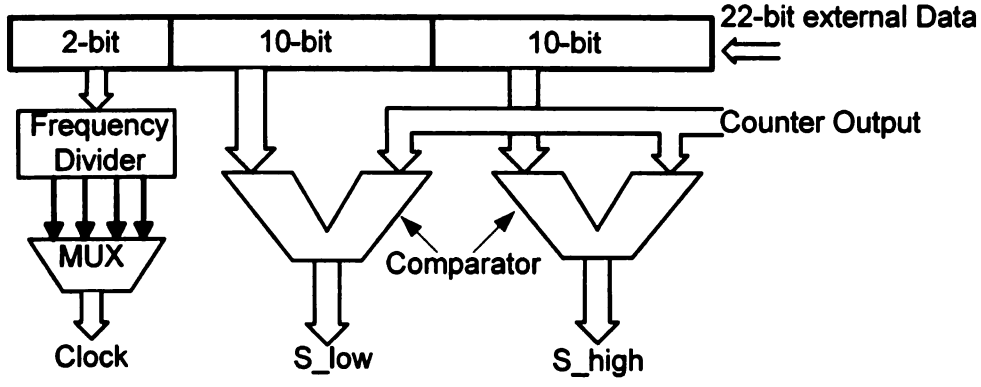

Figure 4.3. Functional diagram of waveform generator block.

design [111-113] that was modified to fit this application. The binary output of the counter is latched and is given to a binary-to-thermometer decoder that generates a thermometric coded digital word. This thermometric code is used by DAC in the next stage and is used to control the switching of DAC analog signal currents. The 4 MSB binary bits of counter output are decoded into a thermometric code that is given to the DAC along with its inverted output, as shown in Figure 4.5, to convert into a discrete analog signal.

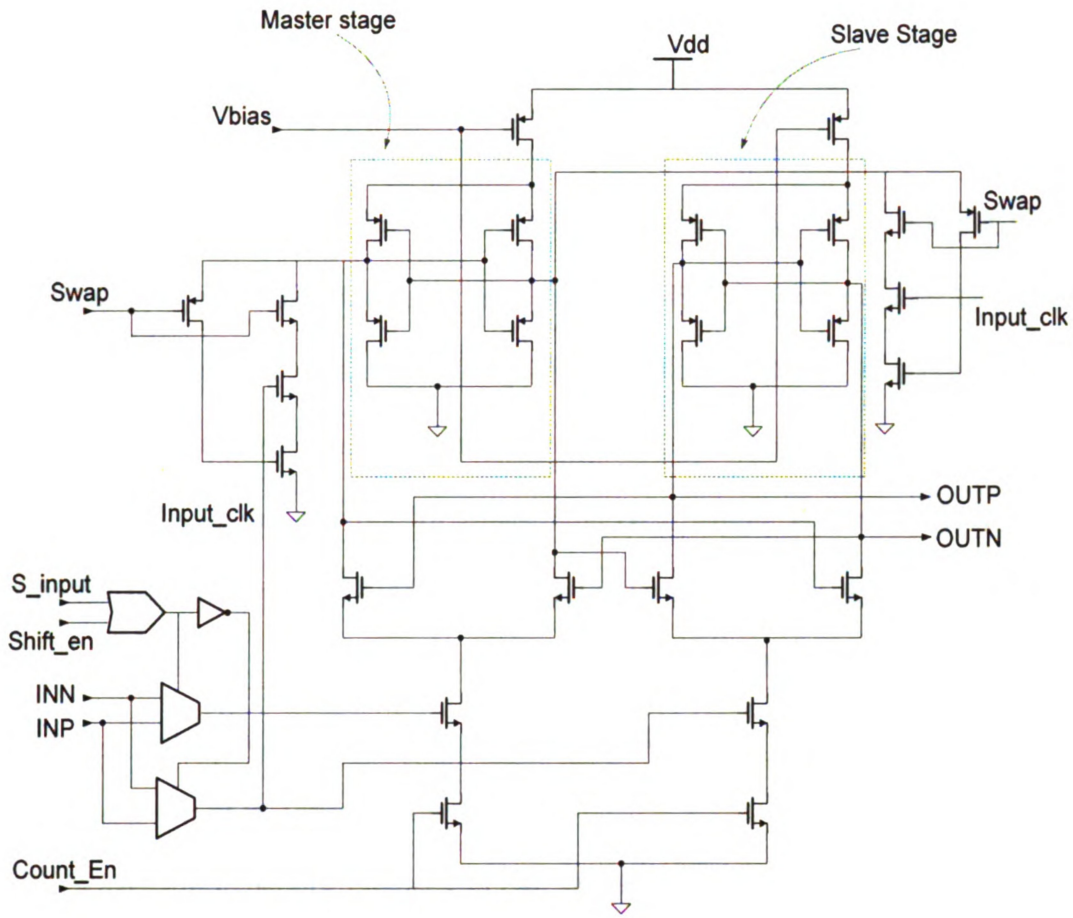

Figure 4.4. Schematic of the bidirectional counter.

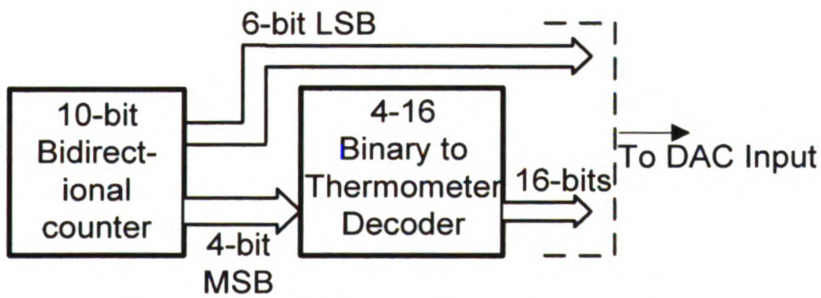

Figure 4.5. Signal flow from counter to DAC.

4.2.3 Digital to Analog Converter(DAC)

The basic function of the DAC is to covert the digital output of the counter into a staircase analog signal that can be applied to the potentiostat. As discussed

above, an 8-bit DAC is sufficient for these waveforms; however, to compensate for process variations in chip fabrication, a 10-bit segmented DAC has been designed to generate a staircase analog signal. It uses a combination of an R-2R ladder network and a current mode thermometer decoder, with the lower six counter bits setting the R-2R ladder and the upper four bits controlling the thermometer decode, as shown in Figure 4.6. This hybrid topology enables the DAC to operate with small currents, improves matching between resistors, and requires less layout area than a full R-2R ladder network for 10-bit. The DAC output is then buffered and sent to the potentiostat. The DAC output spans the range of +1 to -1 relative to analog ground with a step size of 2mV. This provides a stimulus signal up to 2V pk-pk, which is suitable for most electrochemical measurements.

4.2.4 Operation of Waveform Generator

Waveform generator operates in two phases as shown in Figure 4.7. In the first phase, a 22-bit data word is shifted serially into the control block to select scan rate, scan range and type of output signal (waveform). In the second phase, that output signal is generated based on the input signals setup in the first phase.

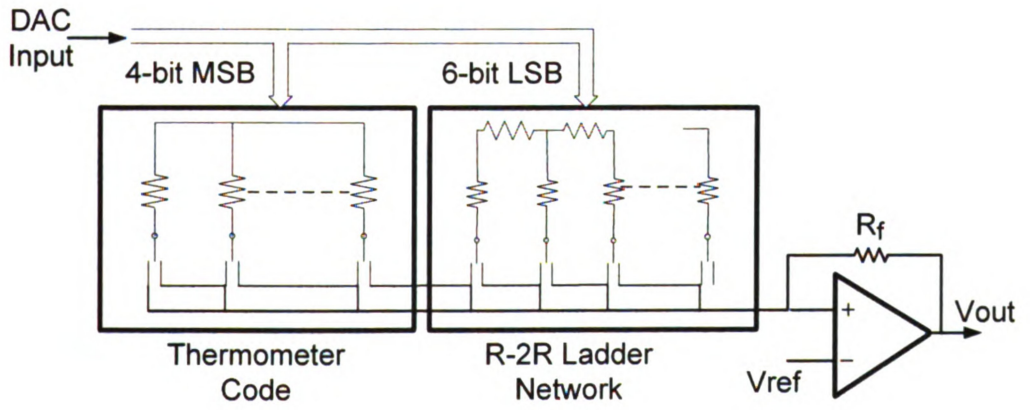

Figure 4.6. Block diagram of hybrid digital to analog converter (DAC) used in waveform generator.

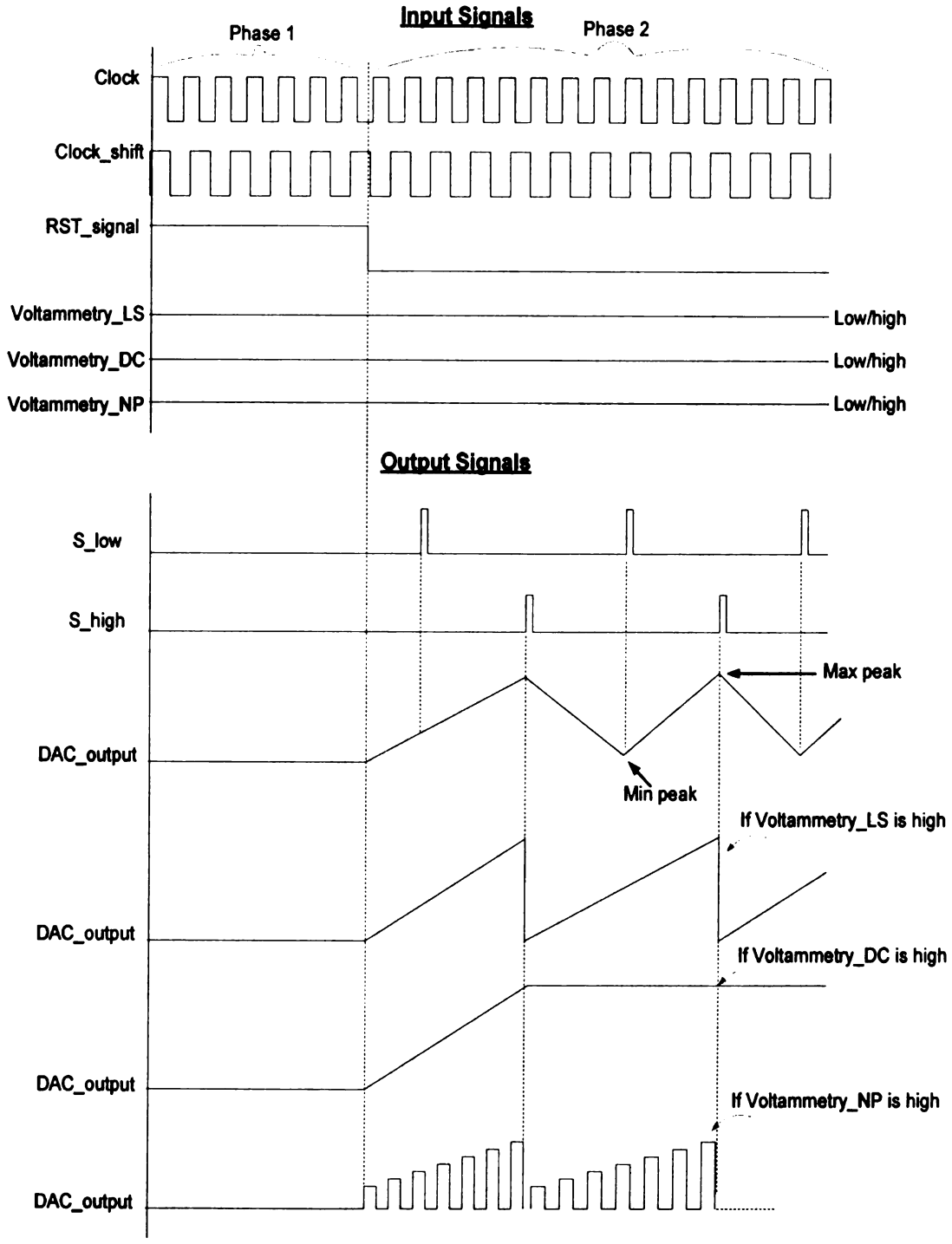

Figure 4.7. Input and output waveforms of waveform generator.

4.3 Single-ended potentiostat

The basic function of an electrochemical potentiostat circuit is to control and maintain the voltage between the working electrode (WE) and the counter electrode

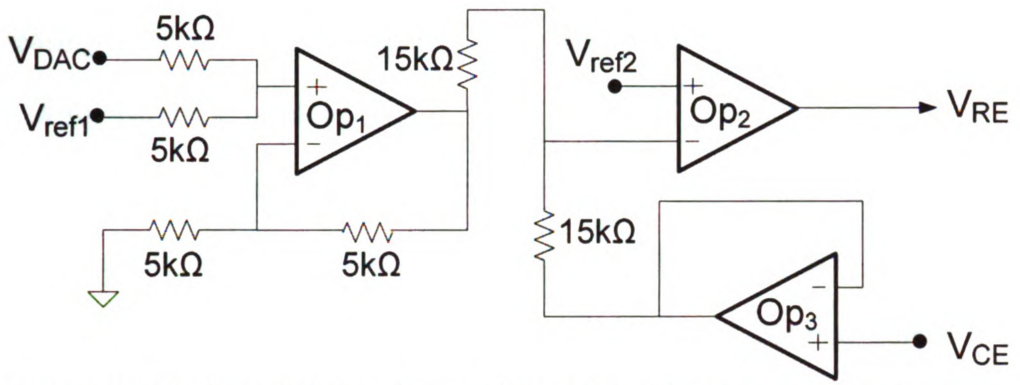

Figure 4.8. Single-ended potentiostat designed for the instrumentation system.

(CE) under varying current conditions. Figure 4.8 shows the schematic diagram of the 3-electrode single-ended potentiostat following the approach in [114]. Output from the waveform generator (V_{DAC}) is level shifted by OP_1 to match the input range of OP_2 by summing it with V_{ref1}.

The output from OP_1, V_{out1}, is given by

$$V_{out1} = \frac{V_{DAC} + V_{ref1}}{2} \tag{4.1}$$

The output of OP_2, which is buffered through negative feedback using OP_3, is connected to the CE. For microscale sensors, it can be assumed that the solution resistance between the reference electrode (RE) and the CE is negligible so that CE and RE are at the same potential. The input of OP_3 is connected to RE and no current flows through the OP_3. The output current resulting from the input stimulus voltage at CE can flow only between CE and WE. V_{ref2} is a DC offset control input

to adjust the scan range. A single bias circuit is used for all three op-amps, decreasing the layout area considerably compared to the potentiostat in [114].

4.4 Amperometric readout circuit

To measure the electrochemical response current at the WE, a capacitive current readout circuit was developed [115]. This circuit was designed by colleagues within our research lab and is included here only to complete the description of the chip. As shown in Figure 4.9, a switched-capacitor (SC) charge integrator converts the current to a voltage. The voltage is sent to a programmable gain amplifier (PGA) with a gain of C_2/C_3, where C_2 is a digitally programmable on-chip capacitor array. The output of the PGA is sampled and held and then fed to an analog-to-digital converter (ADC) after a low pass filter. The non-overlapping clock signals for switches ph_1, ph_2 and ph_3 are generated by an on-chip clock generator block. The output voltage of the current readout circuit is given by:

$$V_{out} = \frac{I_{WE}}{f_s \bullet C_1} \bullet \frac{C_2}{C_3} \tag{4.2}$$

where I_{WE} is the current at the WE and f_s is the frequency of switch ph_2. Thus, the input current range can be adjusted to fit different application through programmable selection of the clock frequency and the PGA gain.

To reduce noise and amplifier offset, correlated double sampling [116] was utilized in the current readout circuit. All switches were realized with minimum size to curtail charge injection. To reduce clock feedthrough errors, dummy switches, with precise time sequence control, were used.

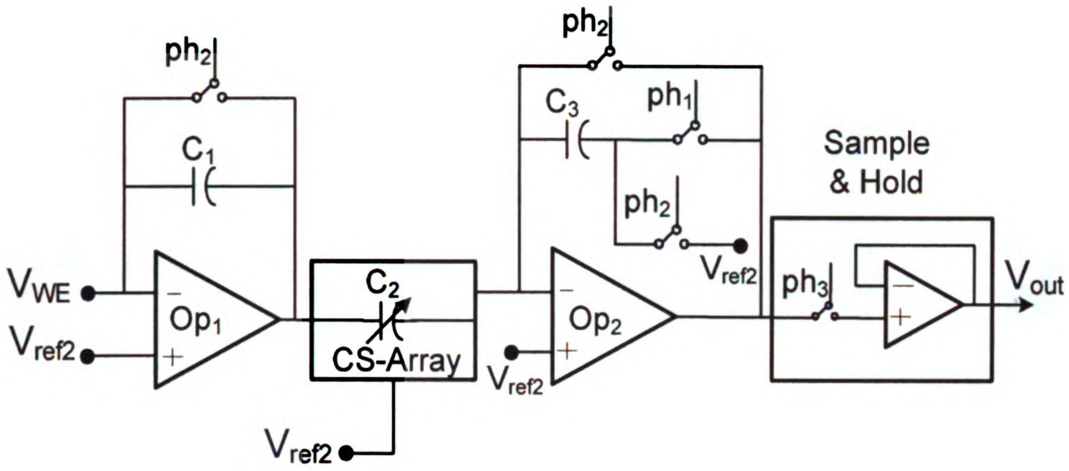

Figure 4.9. Amperometric readout circuit.

4.5 Test Setup

To characterize the functionality of the instrumentation chip, measurements using an electrochemical solution are required. Digital control signals must be generated for the chip along with reference voltages for the potentiostat. In the proposed system, the waveform generator, potentiostat and amperometric readout circuit can each be tested and their functionality can be verified independently. The test setup for the instrumentation chip is shown in Figure 4.10. Test electrodes fabricated on a silicon chip substrate were immersed in the ferro-cyanide (FE_3CN_2) solution, with a copper strip used as the CE and a commercial Ag/AgCl electrode used as the RE. To verify the functionality of chip that is mounted on the test PCB, different waveforms for CV, LSV and constant potential voltammetry were generated, and test electrodes were scanned with different scan rates and scan ranges. A data acquisition card (NI DAQ-6259) was used in conjunction with LabVIEW to generate the control signals for the chip and to acquire the test data at different conditions and waveforms. Test results are presented in Chapter 6.

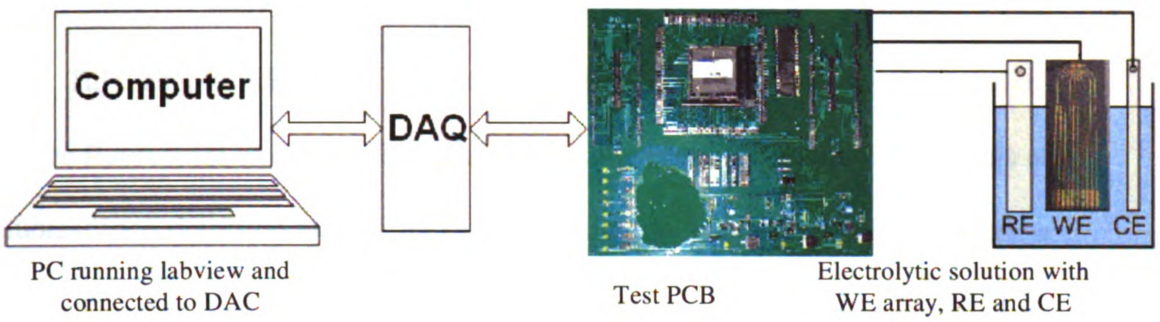

Figure 4.10 Test setup for the instrumentation chip with electrode array.

Chapter 5
CMOS Instrumentation System for Optical Detection

This chapter describes a CMOS optical detection system designed to measure fluorescent emissions from an on-chip biosensor. The main components of a fluorescence detection system include an excitation source, an emission filter, a photodiode, and readout circuit to amplify photodiode currents and generate an output voltage. Usually light detection in CMOS technology is accomplished using a reverse-biased PN junction diode that is comprised of a substrate-to-well junction and a diffusion-in-well junction. Figure 5.1 shows a block diagram of an on-chip optical detection system that includes a fluorescence excitation source, a sensor material that emits fluorescence light, a CMOS IC that includes an integrated filter, and a photo detector with readout circuit to absorb the light energy and further process it. The fluorescence excitation source may be a laser source or LED source to shine light of a specific wavelength on the target/sample containing a fluorophore. The fluorophore emits light at a wavelength that is different from the excitation source. The light energy is detected by the on-chip photodetector and readout circuit within the detector pixel, as shown by the signal flow path in Figure 5.2.

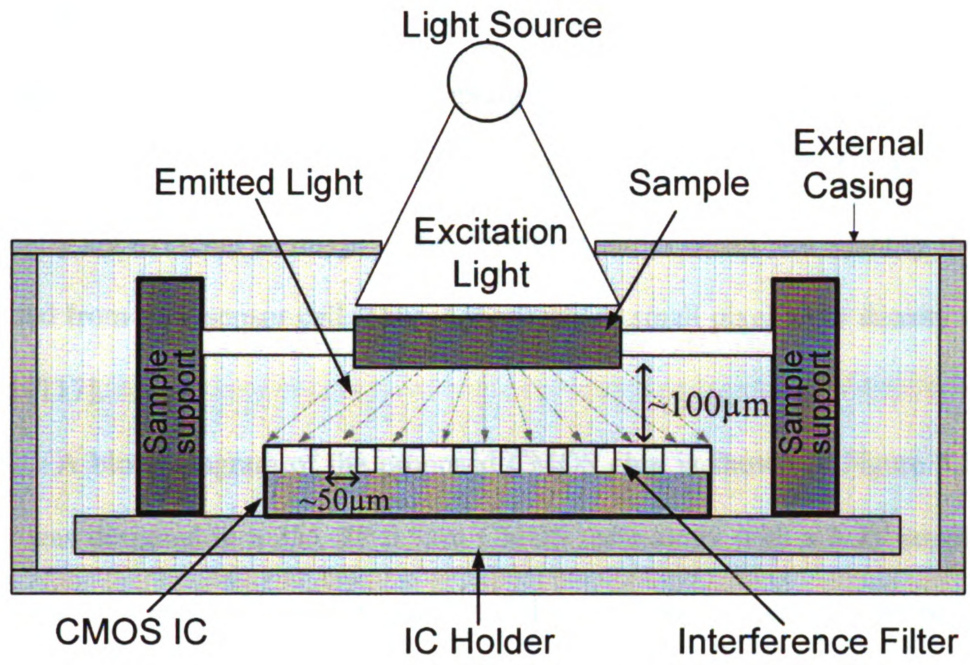

Figure 5.1. Block diagram of CMOS optical detection system

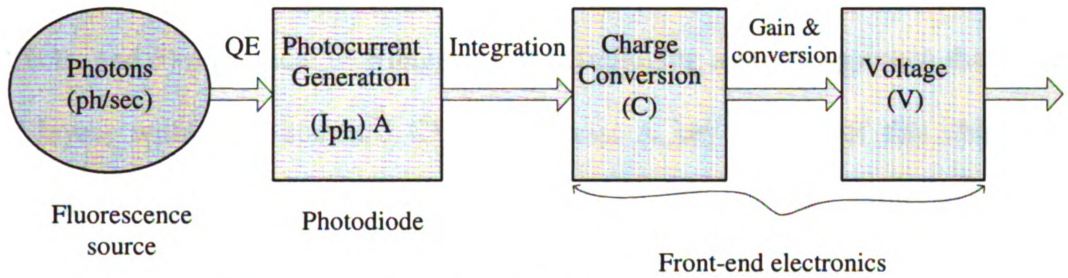

Figure 5.2. Signal flow path from emitted photons to the output.

5.1 Chip Architecture

Many engineering tradeoffs are involved in combining optical and electrochemical detection circuits on a monolithic chip. These tradeoffs affect the fill factor for photodiode and its dynamic range, interference and noise from combined circuit, and orientation of both optical and electrochemical sensor. Design for the optical detection prototype chip was done taking into considerations the requirements of a combined opto-electrochemical detection circuit on a

monolithic chip. For the intended application of biofluorescence assays, i.e. DNA analysis and characterization of membrane proteins including planar bilayer lipid membrane (pBLM) and tethered bilayer lipid membrane (tBLM), the goals is typically not to create an image of the sensor but rather detect and quantify the light emitted from each sensor cell. Thus, a moderate or small pixel array density can be used [117].

A block diagram of the proposed CMOS chip is shown in Figure 5.3. The chip was designed in a 3M, 2P 0.5μm CMOS technology with a 3.3V supply and includes a 4x3 pixel array, with each pixel including: 1) a photodiode to collect photons, 2) a readout circuit to condition the input signals, 3) addressing circuitry to access individual array cells, 4) output buffers to isolate the circuit form loading effects, and 5) an optical interference filter employing a novel approach that relies on layers within the standard CMOS process. A key feature of this chip-scale system compared to other CMOS imager applications is the ability to provide optical filtering within the CMOS chip, which enables biomaterials to be formed on electrodes directly on the chip's surface, as desired for the electrochemical mode of detection in the desired opto-electrochemical system. In the proposed design, each individual pixel is based on a same-sized photodiode, with the same cell size and constant pixel pitch. Compared to traditional CMOS imager applications, a large photodiode detector has been used in order to match the pixel density to the anticipated electrode density of a future combined opto-electrochemical system. This permits each pixel in the array to contain both electrochemical detection circuitry along with a photodiode. Because the electrochemical pixels are large,

~200μm diameter, the photodiode can be quite large to maximize the fill factor of the cell with the added advantage of higher optical sensitivity per pixel.

Because the pixel array is small, optical readout is done per-pixel using a circuit based on a first order ΣΔ ADC so that each pixel can directly convert photo charge to a digital output that can be directly read by an off-chip counter. The advantages of a pixel-level ADC over a chip-level or column-level ADCs include lower noise and low power

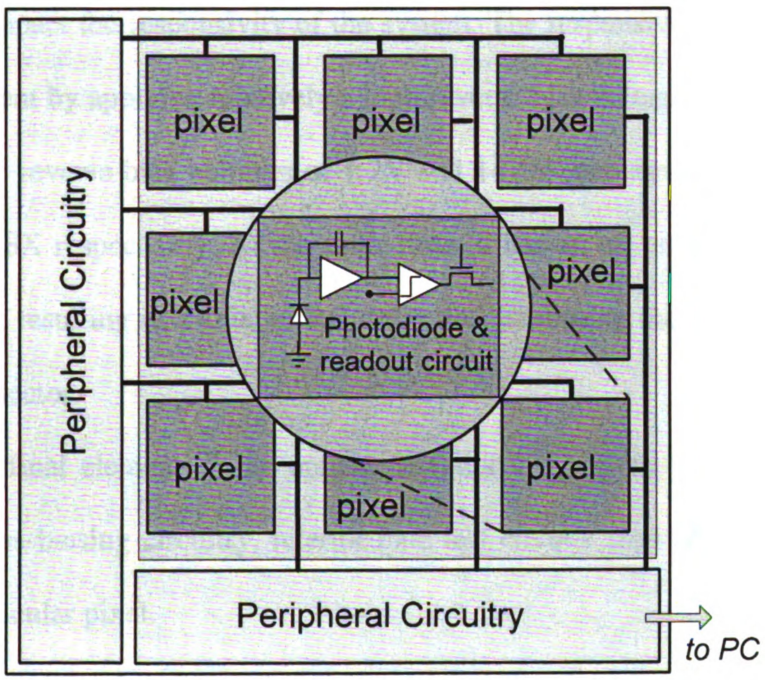

Figure 5.3. Block diagram of the CMOS optical detection chip.

dissipation [118]. Also each pixel can be processed and addressed independently and rapidly without having stringent speed requirements for the circuits within each pixel.

For the optical interference filter, a novel technique has been introduced that utilizes standard CMOS metal layers to realize a diffraction grating. The physical

orientation of the metal layers has been exploited to block excitation light while allowing fluorescent emission light to pass through and be absorbed by the photodiode. This filter is implemented inherently within the CMOS design and does not need any extra post-CMOS processing steps or filtering materials inserted between the biosensor films and the CMOS detectors[87-89]. Although filtering is necessary to ensure the photodiodes respond to fluorescent emissions and are not saturated by background current due to the excitation source, the use of filters does adversely impact the responsivity of the system. The responsivity can be improved to some extent by applying relatively a high reverse bias voltage as implemented in [119] where reverse bias voltages of 1.2V and 14.2V increase the responsivity by 1.6X and 2.8X respectively. At the same time, it has an advantage of lower diode capacitance, resulting in a smaller RC delay and increasing the operating speed of the photodetector.

The final element of the optical detection chip is the peripheral circuitry. This includes biasing circuitry, intermediate test circuits, and address decoders to select a particular pixel.

5.2 Pixel Architecture

The amount of current generated in the photodiode in the pixel mainly depends on the incident light intensity, quantum efficiency (QE) and area of the photodiode. Output voltage from the pixel depends on the photocurrent generated in photodiode, the photodiode's capacitance and the sensitivity of the readout circuit. Design for the pixel architecture takes into considerations the effect of all of these parameters. Each pixel produces a digital output corresponding to the current

generated in the photodiode by incident photons. To match the anticipated structure of the sensor array on the surface of the chip, each pixel consisting of photodiode and front-end readout circuit covers an area of 220x250μm^2. The active photodiode area is 150x200μm^2 and the readout circuit for each pixel covers an area of 70x50μm^2, as shown in Figure 5.4.

5.2.1 Photodiode

A photodiode is the heart of a CMOS image sensor and is used to absorb photons. After an analysis of the different types of photodiodes available in CMOS image sensors including p-n, PIN and avalanche diodes, a standard n-well/p-sub photodiode shown in Figure 5.5(a) was selected. This n-well/p-sub photodiode has better performance in terms of fill factor and quantum efficiency, and it also can be fabricated using the standard CMOS process without requiring any additional processing steps. This photodiode uses a

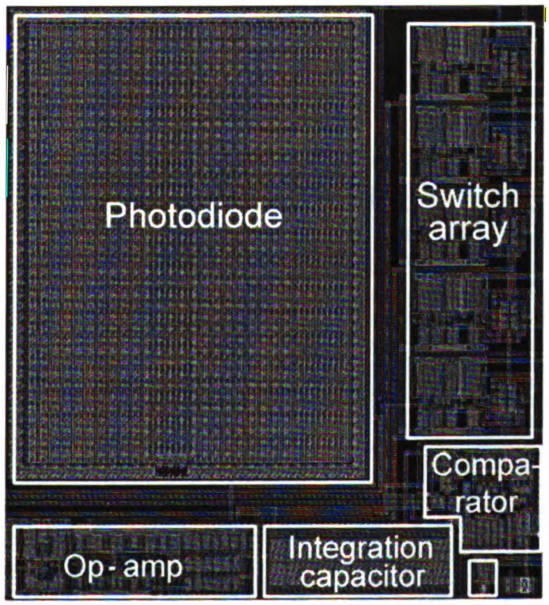

Figure 5.4. Cadence layout of pixel including photodiode & readout circuit.

lightly doped large area n-well diffused into a p-substrate to create a *pn* junction. The *n-well* acts as cathode while p-sub acts as anode. The photodiode is reverse biased to absorb the incident light that carries energy to create electron-hole pairs (EHP) in the depletion region of the diode, resulting in a current flow. This reverse-biased diode current (I_D) is given by

$$I_D = I_S - I_{PH} \tag{5.1}$$

where I_S is the saturation current and I_{PH} is the photocurrent due to the incident light. A layout view of the designed photodiode is shown in Figure 5.5(b).

5.2.2 Front-end Readout Electronics

The basic function of the readout circuit is to collect the output current from photodiode, amplify it, and convert it into a voltage so that it can be processed in a later stage. Different topologies for the front-end readout pixel have been reported taking into considerations the size of pixel array, dark current and thermal noise [78-82]. The chosen readout circuit for the pixel is based on first order sigma-delta

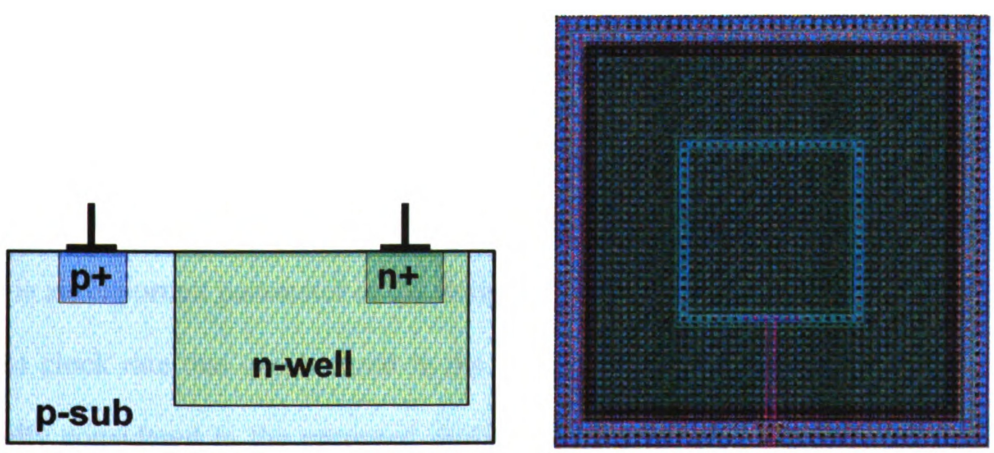

Figure 5.5. (a) Schematic diagram of the photodiode structure, (b) Cadence layout of n-well/p-sub 150x200μm^2 photodiode.

ADC (ΣΔ), as shown in Figure 5.6. Main components of this ΣΔ ADC are 1) an integrator composed of an op- amp and a capacitor in a feedback loop, 2) a comparator with digital output, 3) a clocked latch and 4) a feedback circuit. This ΣΔ ADC has the advantage of low sensitivity to transistor noise and large charge handling capability. Also, noise in the comparator is reduced by the feedback circuit [118].

Figure 5.7 shows the schematic of a high gain operational transconductance amplifier (OTA) with single-ended output used in the integrating amplifier. A single stage amplifier with folded cascode topology was used for a high gain with low demand on hardware area. Also, this cascode gain stage gives immunity to the Miller effect at high frequencies. M1 & M2 form an input differential pair; M3 & M4 form an NMOS current source; M5 & M6 are NMOS cascode transistors to the input differential pair; M7-M10 form a wide-swing cascoded PMOS current source; and M11 is a current source for the differential input pair. To achieve low dark current and high linearity, PMOS transistors are chosen for the differential input stage. The simulated performance of the proposed design shows a DC gain of 95dB and unity gain bandwidth of 25MHz with a phase margin of 50°. Simulated power dissipation of this OTA with a 1pF load is 1mW.

The second main component of the ΣΔ ADC is the comparator. Propagation delay is an important parameter in the design of the comparator because it limits the highest clock rate that can be used in the ADC. The delay in the comparator was carefully considered in the proposed design. The proposed comparator consists of three stages; an input preamplifier, a decision circuit and an output buffer [120], as

shown in Figure 4.8. This topology has the advantage of relatively small propagation delay, in the nanosecond range. The preamplifier consists of a differential amplifier with active loads. Gain of the input stage is set by the transconductance, while input capacitance is determined by the size of input transistors. Decision circuit of the comparator is used to discriminate between signals. This circuit uses positive feedback from cross-gate connection of M7 and M8 to increase the gain of the decision circuit. Output from the decision circuit is given to output buffer which is a self biasing differential amplifier. Output buffer also includes an output inverter as an additional gain stage and to isolate any load capacitance from the self-biasing differential amplifier. Complete schematic of the comparator is shown in Figure 5.8. Output of the comparator is passed through a latch and digital output after passing through output buffer is given to off-chip counter to measure the width of output pulse.

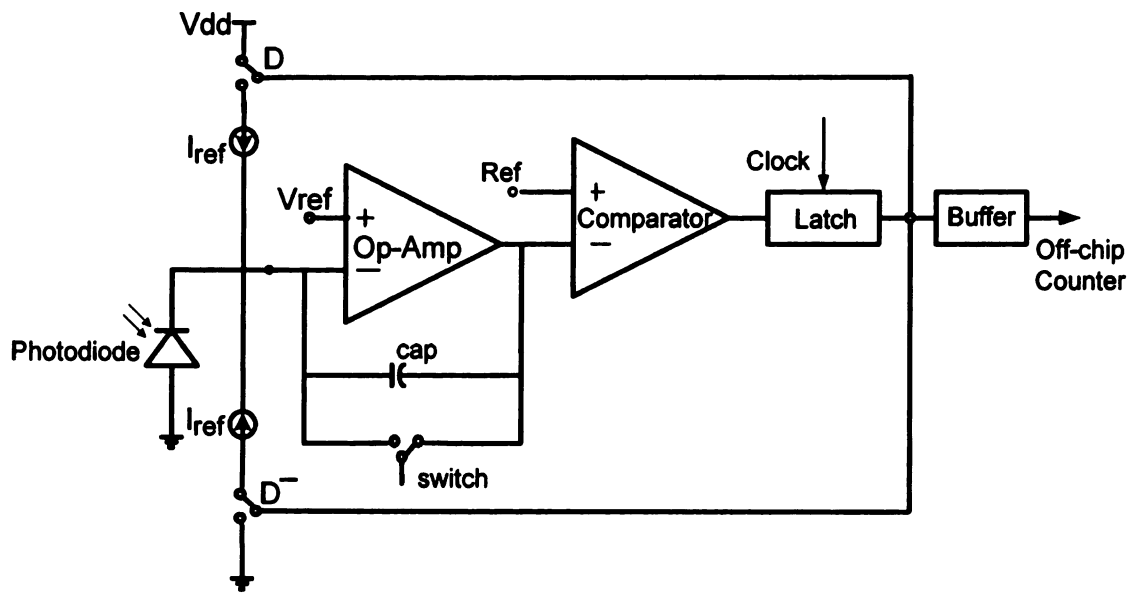

Figure 5.6. Sigma Delta (ΣΔ) ADC used for readout.

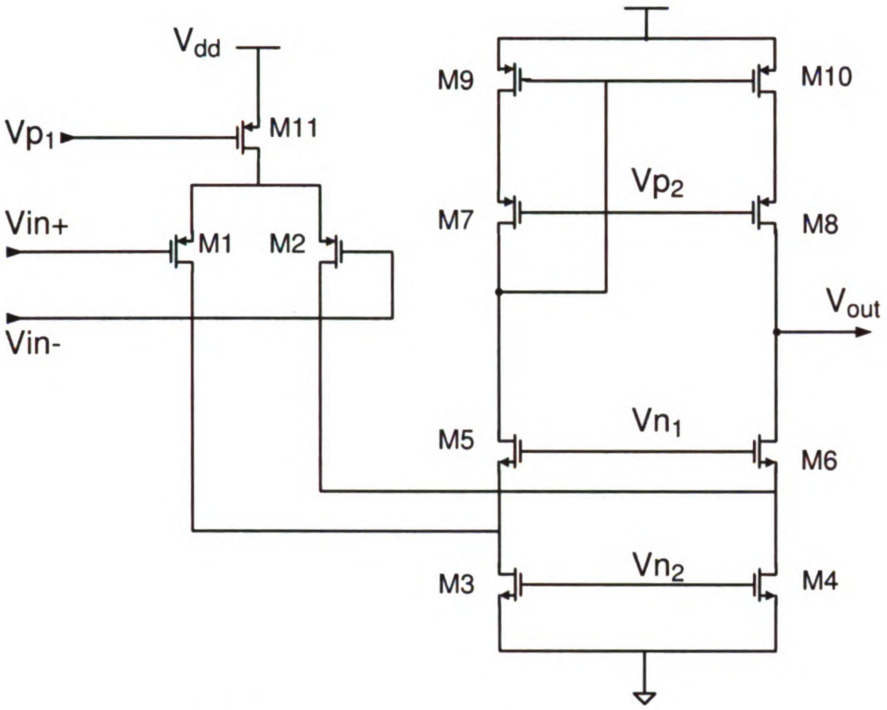

Figure 5.7. Schematic of the folded cascode OTA.

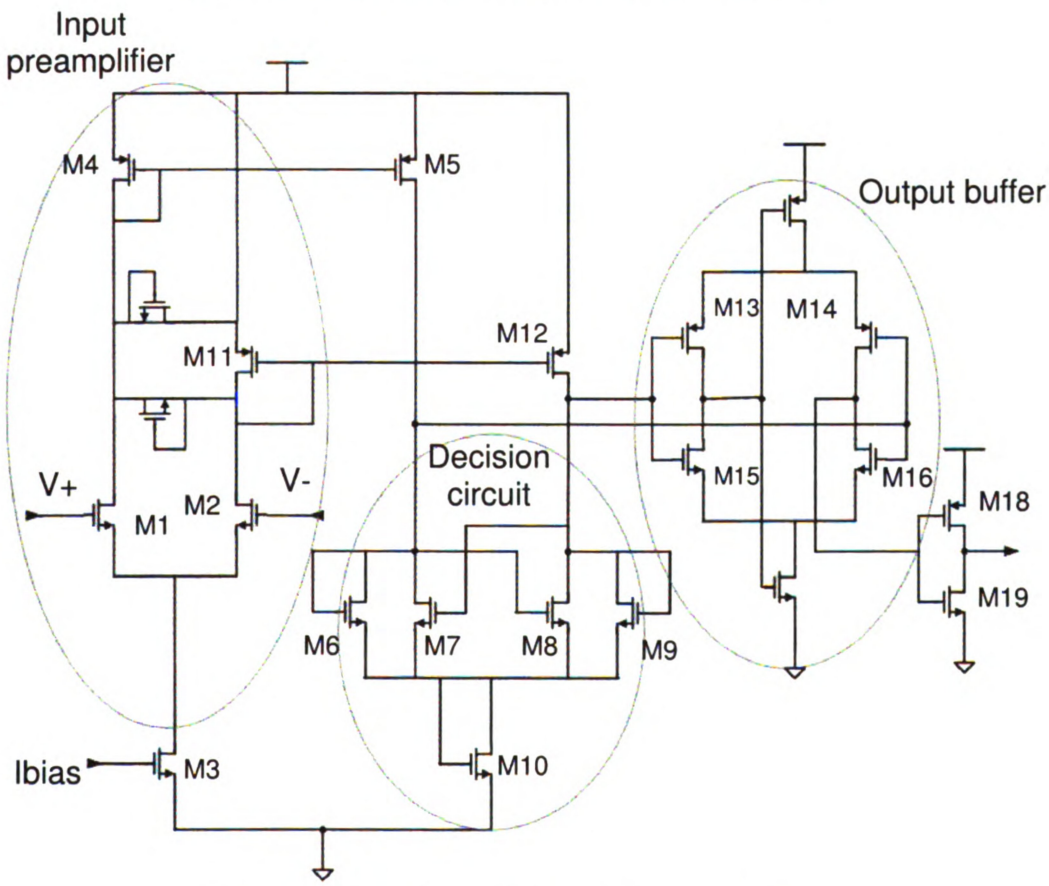

Figure 5.8. Schematic of the voltage comparator.

5.3 On-chip Filter

5.3.1 Introduction

The basic function of the on-chip interference filter is to selectively inhibit transmission of the excitation light and allow the transmission of light emitted from the fluorophore in bilipid membrane (BLM). Emitted light from fluorophore has a longer wavelength than the excitation light due to stokes shift and this change in wavelength is exploited to get the required wavelength of light emitted from fluorophore. The amount of change in wavelength depends on the type fluorophore used in the analysis. In many fluorescent systems, the filter is implemented using a specific material, inserted between the fluorophore and the detector that allows transmission of only a specific wavelength of light. Traditionally, filters that have been integrated on CMOS ICs rely on post-CMOS processing to build optical filters on the top of the chip. However, for a combined opto-electrochemical system post-CMOS processing is not feasible to integrate the filter as biomembranes are stored in fluidic environment

5.3.2 Design Methodology

In the proposed optical detection system, a novel technique has been developed for the on-chip filter by using the metal layers in the standard CMOS fabrication process to create an interference filter without any post-CMOS processing. Metal inherently blocks the visible light to a large extent based on its permittivity and this property of metal has been used in the proposed design of filter. The placement, width and horizontal gap between the CMOS metal layers

have been manipulated to create a multi-slit diffraction grating that passes the emission light and blocks the excitation light from the light source.

A conceptual block diagram of the on-chip filter that uses CMOS metal layers as a diffraction grating in C5N process is shown in Figure 5.9. The top metal layer, M3, is used as a transmission grating with openings between M3 strips acting as slits with constant widths and constant separations. Similarly, the M2 layer is used as a reflecting or blocking grating. The third metal layer M1 is used for an improvement in the selectivity of the filter. Also, M1 serves the purpose of blocking additional amount of light if passed though M2 layer because of its permittivity.

Each slit in M3 is considered to be a point source generating the same flux intensity distribution. When incident light is perpendicular to the diffraction grating, the angle of diffraction for bright regions of light is given by the diffraction grating equation

$$d \sin \theta_m = m\lambda \tag{5.2}$$

where d is the distance between the centers of adjacent slits, λ is the wavelength of incident light, θ_m is the angle of diffraction, and m is an integer denoting diffraction or spectral order. Equation (5.2) shows that the angle of diffraction increases with increase in wavelength.

This multi-slit grating can be considered as an array of N identical slits, each slit having a width x and equally spaced. Calculations were done for the above mentioned model (figure 5.9) and based on some ideal assumptions with unity diffraction order i.e. m=1. Incident light was assumed to be perpendicular to the photodiode. The reason for this assumption was that, in the proposed detection

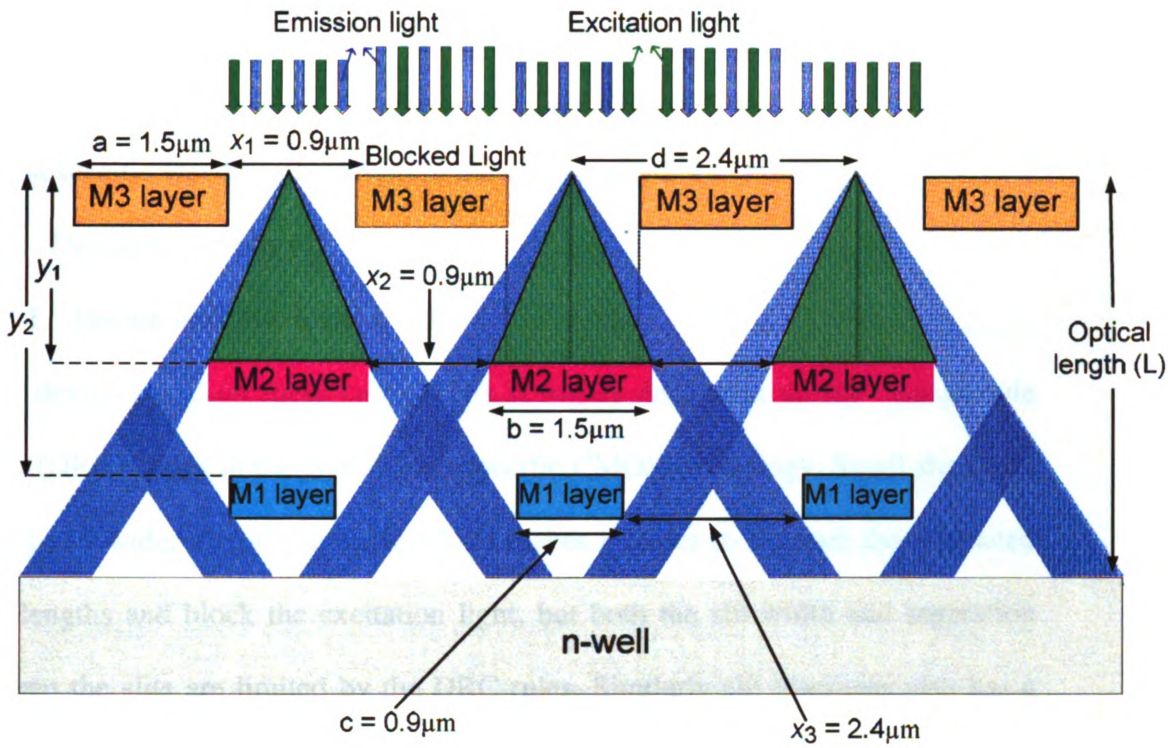

Figure 5.9. Conceptual block diagram of a CMOS optical interference filter.

system light source is too close to the photodetector and also incident light at the edges of slit would be blocked by the slit thickness to some extent.

From equation (2) and the trigonometric relation of the dispersed angle, the following equation is derived

$$\tan\theta = \frac{x}{L} \tag{5.3}$$

where L is the optical path length and x is the distance along the surface of the photodiode. Equations (2) and (3) relate the dispersed distance, x, to the wavelength λ of incident light.

Depending on the fluorophore, the Stokes shift generally ranges between 10nm and 150nm [121]. Calculations were done using the above equations for the visible range of light (320-780nm) to determine the angle of dispersion. Based on

the diffraction angle and vertical distance between M3, M2 and M1 layers, placement and width of M2 and M1 layer strips was determined that is required to block a specific wavelength of light in the visible range.

5.3.3 Design Constraints

5.3.3.1 Design and fabrication rules

Filter design based on these calculations is highly dependent on the "design rule check (DRC)" rules in the layout for a specific CMOS technology. Small slit width results in a wider diffraction angle which makes it easier to separate the diffracted wavelengths and block the excitation light, but both the slit width and separation between the slits are limited by the DRC rules. Similarly slit thickness also has a significant effect on the transmission of light which is not considered in Equation 5.2 to determine the diffraction angle. Due to this thickness, incident light with larger diffraction angle is also blocked. Thickness of different metal layers i.e. M1, M2, M3 and vertical distance between these metal layers i.e. y_1, y_2 and substrate L are governed by the specific CMOS process technology and cannot be revealed because of the proprietary rights. Thus, there is a limitation in the transmission of emission wavelength range and an effect on selectivity of the filter. Taking into considerations the DRC rules, optimal wavelength of light calculated for C5N process was approximately 600nm-780nm, while thickness of metal layers has an additional effect on the calculated range. Table. I shows an example of the limitation of selecting wavelength using DRC rules for C5N process. This table shows the calculated diffraction angle "θ" with a slit width "x_1" of 0.9μm for excitation light (600nm), minimum (610nm) and maximum emission light (750nm)

along with M2 stripes width "b" and opening between M2 stripes (slit width) "x_2" to allow the emission light. However, due to DRC rules for C5N CMOS process, minimum width of M2 layer used was 1.2μm with a minimum opening of 0.9μm between M2 stripes which limits the minimum wavelength to be transmitted through opening between M2 stripes. Results of the effect of these DRC limitations and metal thickness have been presented in chapter 6 which conclude that an excitation wavelength less than 730nm to be blocked by M2 stripe width. For advanced CMOS processes that uses less metal widths because of different DRC rules, diffracted angle increases for the same wavelength of light and also the transmitted wavelength range is also increased as presented in *Section 5.3.4.*

Also proper placement of M1 layer can increase the performance of filter by blocking a percentage of excitation light that is transmitted due to the permittivity of M2 layer and also increasing the selectivity of the required wavelength of light.

TABLE I. CALCULATED DIFFRACTION ANGLE FOR EXCITATION AND EMISSION LIGHT FROM FLUORPHORE AND M2 LAYER WIDTH AND SEPARATION BETWEEN M2 STRIPS FOR C5N PROCESS

Wavelength λ	**Diffraction angle (θ)**	**M2 layer width (b)**	**M2 layer opening (x_2)**
600nm (Excitation light)	14.48°	0.98μm(to block the 600nm light)	~0.27μm (to transmit light between 610nm-750nm)
610nm (minimum emitted light)	14.72°		
750nm (maximum emitted light)	18.21°		

5.3.3.2 Filter Transmission Factor

Due to use of metal layers on the top surface of photodiode for filter and limitation from DRC of C5N CMOS process, amount of transmitted light on the photodiode is also affected. In the proposed technique incident light (both excitation and emission) is alternately blocked and allowed by the top metal layer M3. Fill transmission factor was determined based on some assumptions and a set of following equations.

Assuming I as excitation light from the light source and with E as emission light from the fluorophore distributed in all directions while X is the incident emission light on top metal layer of filter. As emission light intensity is always less than by some factor and also background light has also an effect on emission light, so emission light from fluorophore is given by

$$E1 = I \bullet \alpha_F \bullet \alpha_{background} \tag{5.4}$$

where α_F is the emission factor from fluorescence and $\alpha_{background}$ is the background light factor. As photodetector is placed only under the fluorophore so half of the emission light is incident on photodiode area an is given by

$$X_1 = \frac{1}{2} E_1 \tag{5.5}$$

where X_1 is the emission light incident on photodiode. As filter is covered by alternating layers of top metal layer M3 and it was determined from the covered area that **35%** of X_1 is transmitted through the top metal layer. Assuming 50% of emission light incident on the pixel, calculated transmitted light through the filter is **9%** of emitted light from fluorophore **for C5N process**. For IBM 0.13μm process

which uses less metal width at the top, fill transmission factor calculated is **20%** using the same set of equations as used for C5N process.

Similarly, analysis was performed to determine the minimum amount of excitation light that can be quantified by the readout circuit by using the following equation

$$I_p = R\left(\frac{N_p E_p}{t}\right) \tag{5.6}$$

where I_p is the photonic current that can be detected by readout circuit, R is the responsivity of photodiode, N_p is the number of photons and E_p is the energy of photon.

5.3.3.3 Process Variations

Filter design is also constrained by the process variations of fabrication process. As a result, metal widths may change that have an impact on the functionality and performance of filter. An analysis has been done to determine the effect of process variations of on the functionality of filter. A process variation of 15% for metal widths was assumed for simulations. Details of this analysis have been presented in chapter 6.

5.3.4 Effect of CMOS technology feature size

For C5N process only 3 metal layers are allowed but for advanced CMOS technologies e.g. 0.35µm, 0.18 µm process, additional metal layers can be included in the layout and also these processes have different DRC rules which can be manipulated to increase the functionality and selectivity of the filter. Smaller slit width and separation can increase the diffraction angle, which makes it easier for

the filter to block/allow the incident light. To determine the effect of extra metal layers and advanced CMOS technologies, filter design was also implemented in IBM 0.13μm CMRF8SF process. Calculations were done for the diffraction angle and width of metal layers for the visible range of light. Table. II shows the diffraction angle for the same wavelengths of light used in C5N process. For IBM 0.13μm process four metal layers i.e. M1, M2, M3 and MG were used with slit width for the top layer used was 0.6μm and a slit separation of 0.8μm. It is evident from the Table II that for the same wavelength of light diffraction angle is wider and separated which makes it easier for metal layers to discriminate between wavelengths. The effect of these extra metal layers on the selectivity of filter for IBM 0.13μm process has been demonstrated in Chapter 6.

TABLE II. DIFFRACTION ANGLE FOR EXCITATION AND EMISSION LIGHT FROM FLUORPHORE FOR IBM 0.13μM CMFRF8SF PROCESS

Wavelength (λ)	**Diffraction angle** ($\theta°$)
600nm (Excitation light)	25.38°
610nm (minimum emitted light)	25.83°
750nm (maximum emitted light)	32.39°

5.4 Physical design

The optical detection circuit was implemented on a 1.5x1.5mm^2 chip in a 2P, 3M 0.5μm CMOS process, as shown in Figure 5.10. The diffraction grating filter was implemented using M1, M2 and M3 layers within the active photodiode area. Due to fabrication process restrictions vertical distance between the layers cannot be changed. Similarly, the width of metal strips and the horizontal distance between metal strips is also constrained by the minimum design rules for a specific

CMOS technology. To permit experimental evaluation of different filter design parameters, the diffraction grating over each photodiode in the array utilize different slit widths and slit separations. Layout for the readout and addressing circuitry was done using only M1 and M2 layers. Readout circuits have been fully covered by the top CMOS metal layer M3 blocking the light to protect the circuits from laser light that can change the properties of the circuits.

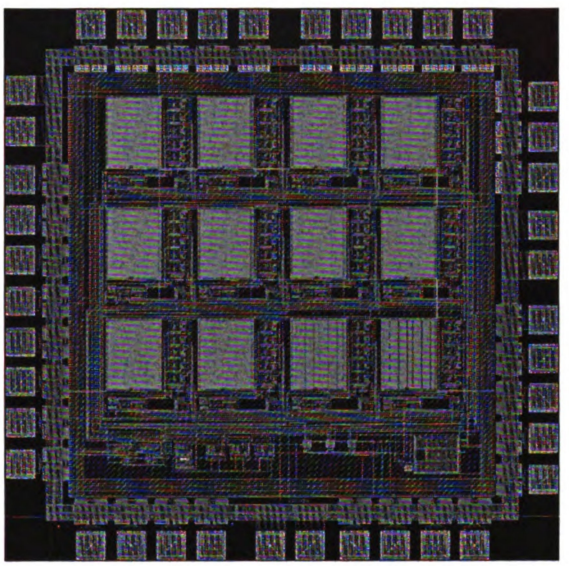

Figure 5.10. Cadence layout of the 1.5x1.5mm^2 optical detection chip.

5.5 Summary

An optical detection system has been presented for fluorescence detection with in-pixel readout. Intended application of this system is characterization of biofluorescence assays. Main components of this system are photodiode, on-chip filter and readout circuit. An n-well/p-sub photodiode is used to absorb photons. The in-pixel readout is based on a first order ΣΔ ADC. A novel technique is used for interference filter by exploiting the orientation of metal layers in layout that

does not require any post-CMOS processing. Design of this optical detection system was done to meet the demands of on-chip opto-electrochemical sensor array. The first prototype chip was designed in 2P, 3M 0.5μm CMOS process.

Chapter 6
Simulation and Experimental Results

The autonomous on-chip multimode voltammetry microsystem (Chapter 4) and optical detection circuit (Chapter 5) were developed to demonstrate the feasibility of an opto-electrochemical detection microsystem and to explore the relevant analog/mixed signal IC design methodology for such a combined system on a monolithic chip with different functionalities. Both circuits were fabricated in AMI 0.5μm C5N CMOS technology using a 3.3V power supply. This chapter presents the simulation and experimental test results of the proposed design and fabricated chips respectively and an analysis of their functionality and performances.

6.1 Measurement of Multi-mode Voltammetry CMOS Microsystem

Figure 6.1 shows the die photograph of the 3mm X 3mm prototype multimode voltammetry CMOS IC. A 2 x 2 array of working electrodes (WE), with single counter electrode (CE) and reference electrode (RE) are integrated on IC for on-chip biosensor measurements. Three main components of the microsystem i.e. waveform generator, 2 x 2 potentiostat array and readout circuit were tested individually.

6.1.1 Waveform generator

6.1.1.1 Test Setup

To verify the functionality of programmable waveform generator, a test setup comprised of the instrumentation chip, and a PC with a DAQ card NI-USB 6259 and running a LabVIEW user interface was prepared as shown in Figure 6.2.

This LabVIEW software is used to generate the digital control signals and also to acquire data from the CMOS chip.

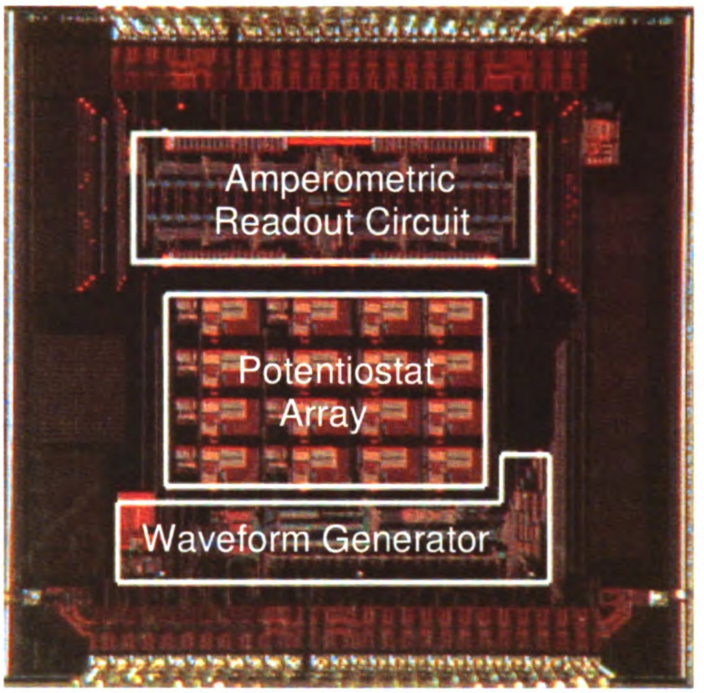

Figure 6.1. Die photograph of 3mm x 3mm multi-mode voltammetry system.

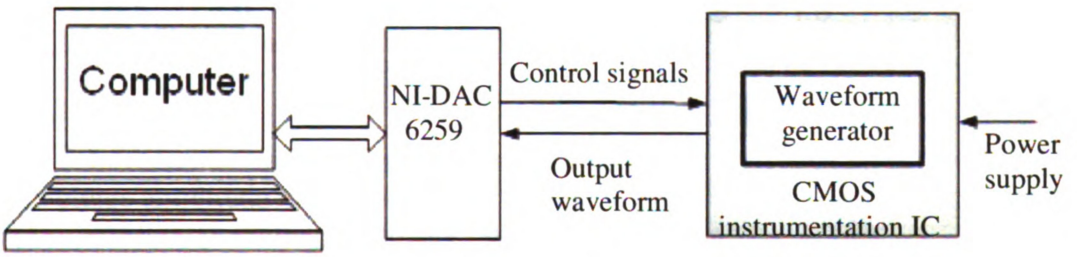

Figure 6.2. Experimental test setup for the on-chip waveform generator.

6.1.1.2 Test results

Figure 6.3 shows simulated output signals from the waveform generator for each of the four implemented waveform modes. All signals were generated under the same parameters with a scan range of 2V (max) and scan rate of 4V/sec using a 2 kHz input master clock. This translates to amplitude of 2Vpk-pk and output

frequency of 1Hz. The characteristics of the waveform generator are summarized in Table III.

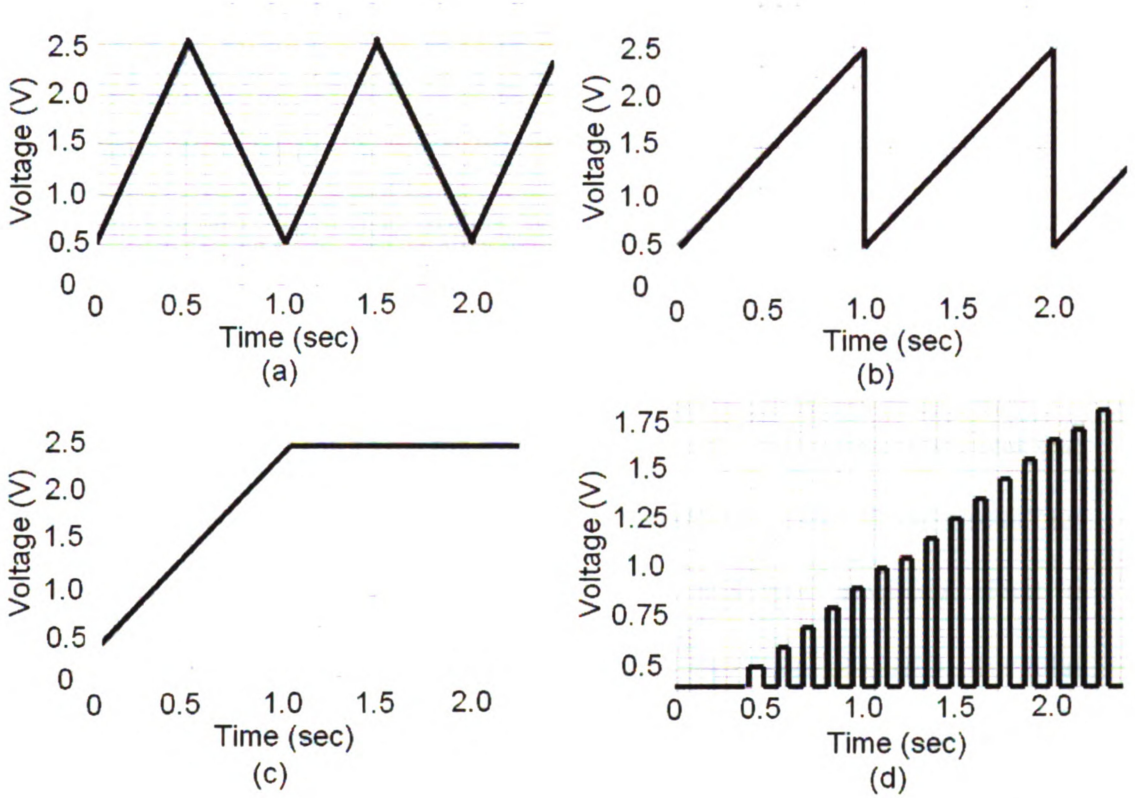

Figure. 6.3. Simulation results for the waveform generator with time on the x-axis and voltage amplitude on the y-axis. (a) triangular signal, (b) linear sweep, (c) constant potential, (d) square pulse with increasing amplitude.

TABLE III. WAVEFORM GENERATOR CHARACTERISTICS

Area	$0.44mm^2$
DAC Resolution	10 bit
Scan range	0- 2V pk-pk, 10-bits
Scan rate	1mV/sec-400V/sec
Step size	2mV
Power consumption	0.15mW

6.1.2 Potentiostat

6.1.2.1 Test Setup

To verify the electrochemical measurement capability of potentiostat, the test setup that was prepared, comprised of the instrumentation chip and PC with a DAQ card (NI-6259) running the LabVIEW software. Initially the potentiostat circuit was characterized without the electrochemical setup using an external waveform generator (Tabor Electronics, Waveform Generator-WW5062).

For testing with electrochemical setup a typical electrolyte solution consisting of 0.1M (molar) potassium ferrocyanide and 1M potassium chloride buffer was prepared. Test setup for on-chip potentiostat with electrochemical test setup is shown in Figure 6.4. Measurements were performed at 25°C and a scan rate of 100mV-s^{-1} with a liquid junction Ag/AgCl reference electrode. First a commercial instrument (CH Instruments 700C) was used to take a cyclic voltammetry (CV) measurement with an on-chip WE. The instrumentation chip was then connected to an external electrochemical cell composed of commercial components, and a CV measurement was performed using on-chip electronics.

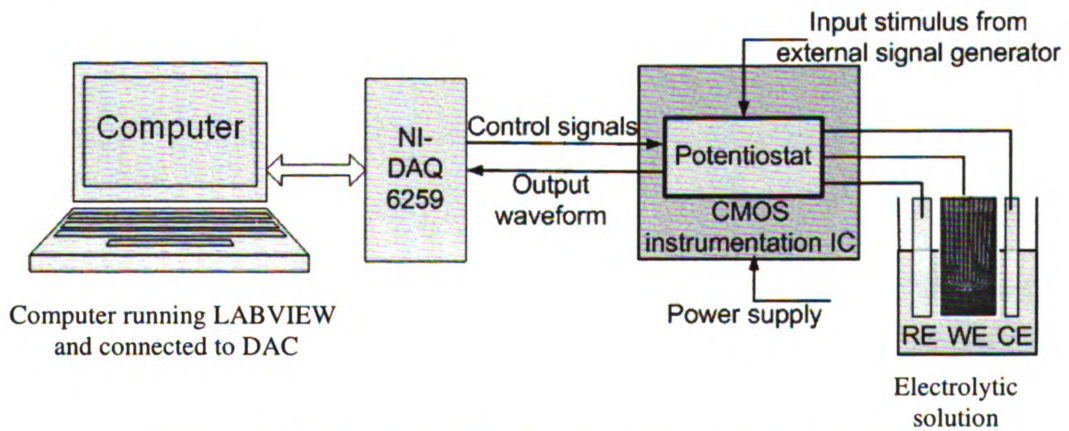

Figure 6.4 Experimental test setup for on-chip potentiostat.

6.1.2.2 Test Results

A series of tests were performed to compare the functionality of the commercial potentiostat with on-chip potentiostat.

Test results of the potentiostat with electrochemical test setup are shown in **Figure 6.5**. Figure 6.5(a) show the results of cyclic voltammetry (CV) test using the commercial potentiostat (CH Instruments 700C) at a temperature of 25℃ with a scan range of 0.4V and scan rate of 100mV/sec, while Figure 6.5(b) shows the result of on-chip potentiostat for a CV curve with oxidation-reduction peak separation of 0.14V. This compares well with measurements of the same electrochemical cell using commercial instrument, where peak separations of 0.1~0.15V were typically observed. The x-axis values for Figures 6.5(a) and 6.5(b) are different because of internal biasing of the CMOS potentiostat.

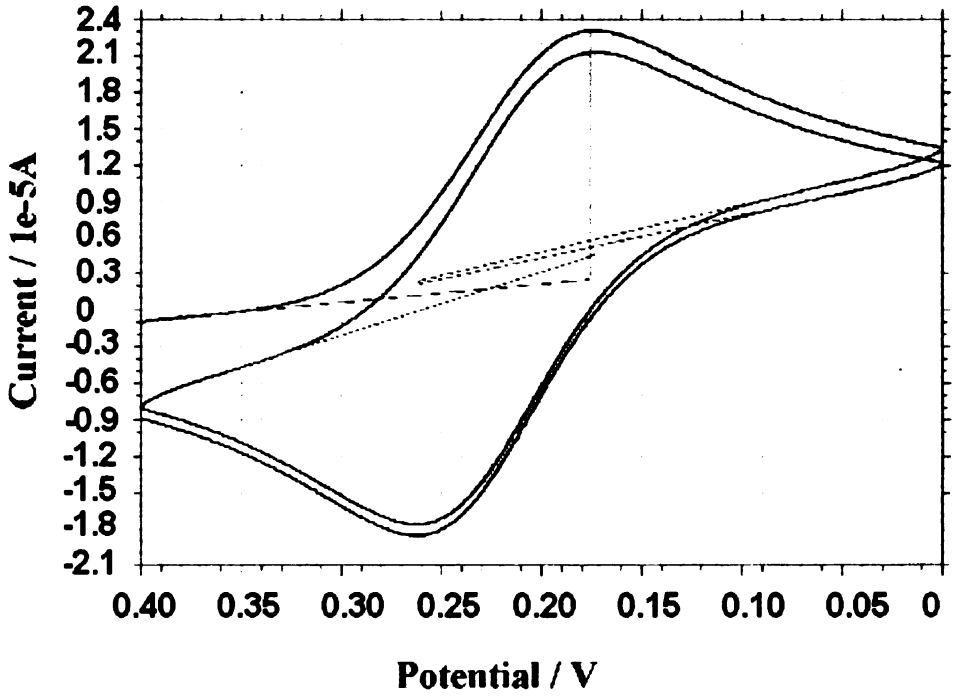

(a)

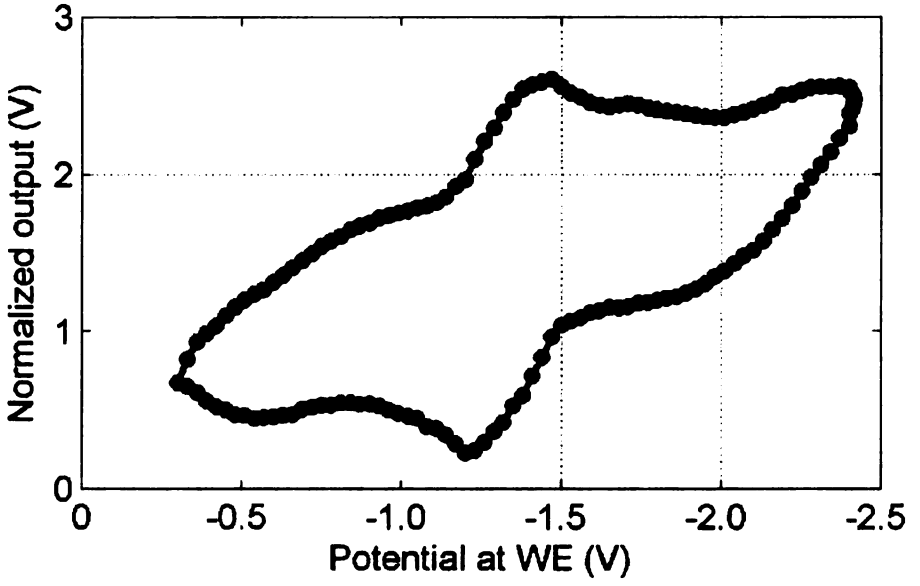

(b)

Figure. 6.5 CV measurement of 0.1M potassium ferrocyanide (K_4•$3H_2O$) for on-chip electrode (a) using commercial instruments showing a peak separation of ~0.10V, (b) using on-chip potentiostat showing a peak separation of ~0.14V.

6.1.3 Amperometric readout circuit

Amperometric readout circuit [115] was also tested to check the functionality and performance of the circuit. This amperometric circuit was designed and tested by fellow student Xiaowen Liu, at AMSaC lab, Michigan State University. The circuit was tested using DAQ card (NI-6259) and PC running the LabVIEW software to generate control signals for the circuit and also acquire the output signal from the chip. **Figure 6.6** shows the LABVIEW test program interface to test the functionality of amperometric readout circuit. A source meter was used to sweep the working electrode (WE) current from 1μA to 9μA. As shown in Figure 6.7 for a 100 kHz sampling clock, the circuit provides a linear output voltage over a wide current range; it was found to perform correctly with inputs up to 100μA. Thus, the amperometric readout circuit supports about 180dB dynamic range by changing the frequency of the sampling clock and the gain of the PGA.

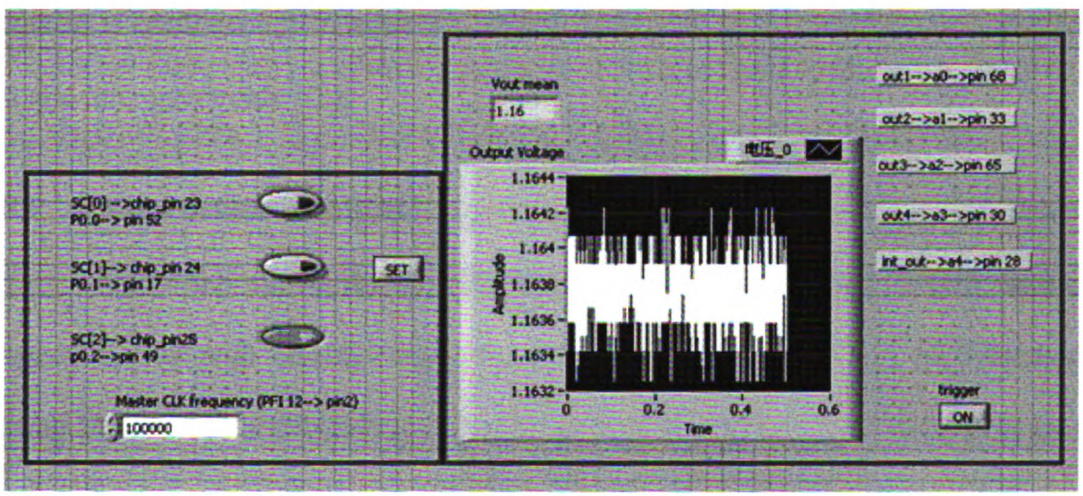

Fig 6.6 LABVIEW test program interface to test the functionality of amperometric readout circuit

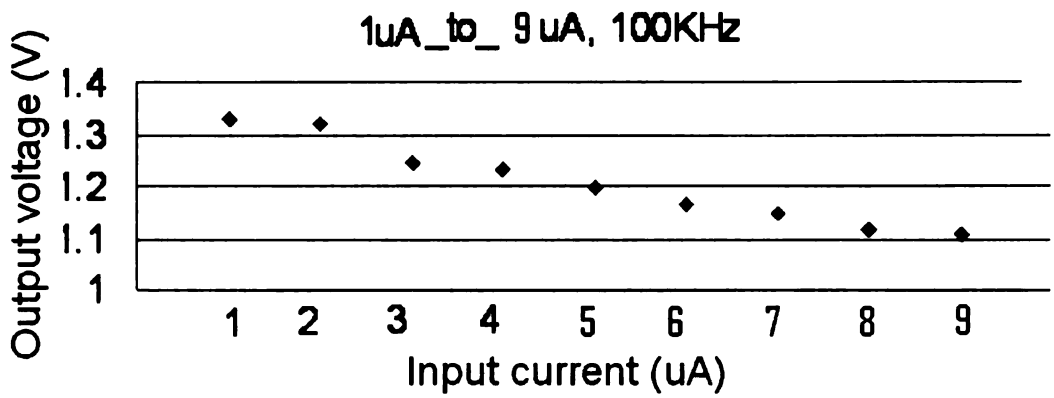

Figure 6.7 Current readout circuit results for input current from 1μA to 9μA.

6.1.4 Discussion

The simulation results of the on-chip waveform generator and experimental results from potentiostat and amperometric readout circuit demonstrate that the circuits developed in this dissertation can be used to characterize membrane proteins using a platform that uses multiple voltammetric techniques i.e. CV, LSV, constant potential and normal pulse voltammetry (NPV). Also design of these circuits is small enough to support a large array of such sensors with (or on top of) a single microelectronic chip.

6.2 Optical detection system

Figure 6.8 shows the cadence layout of 1.5mm x 1.5mm CMOS optical detection chip with on-chip filter. Readout circuit in the chip was implemented using M1 and M2 layers and was later covered by M3 layer in the layout to protect the circuit from the adverse effects of laser light that may change the characteristics of the readout circuit. Die photograph of the fabricated chip with readout circuit covered with M3 layer is shown in Figure 6.9.

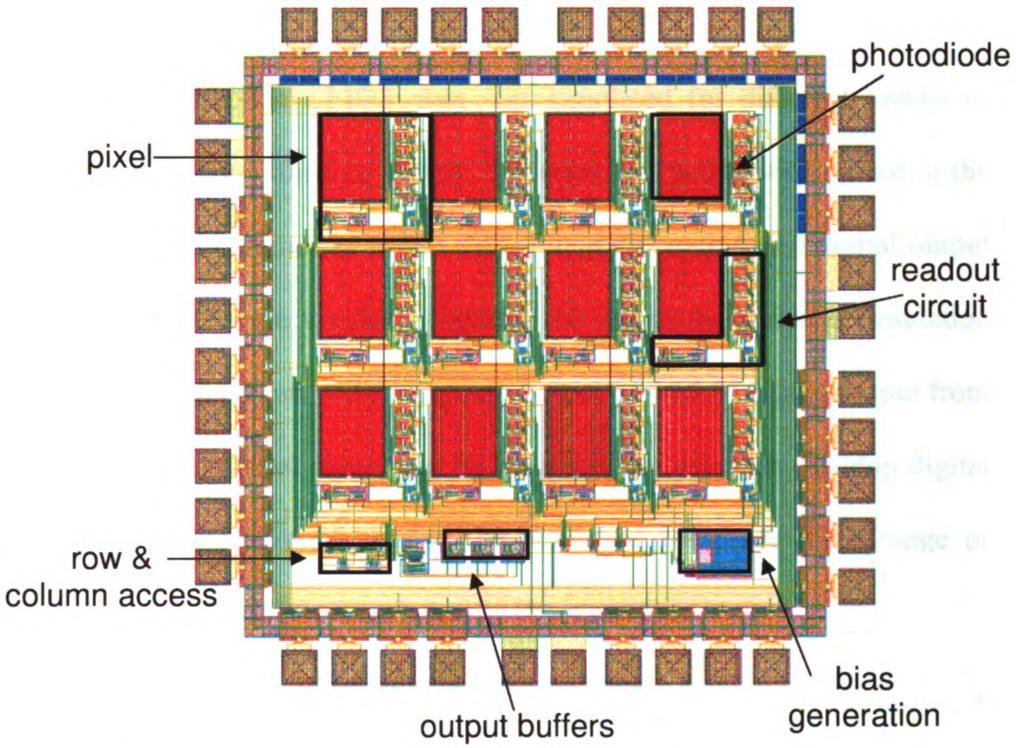

Figure 6.8 Cadence layout of CMOS optical detection IC.

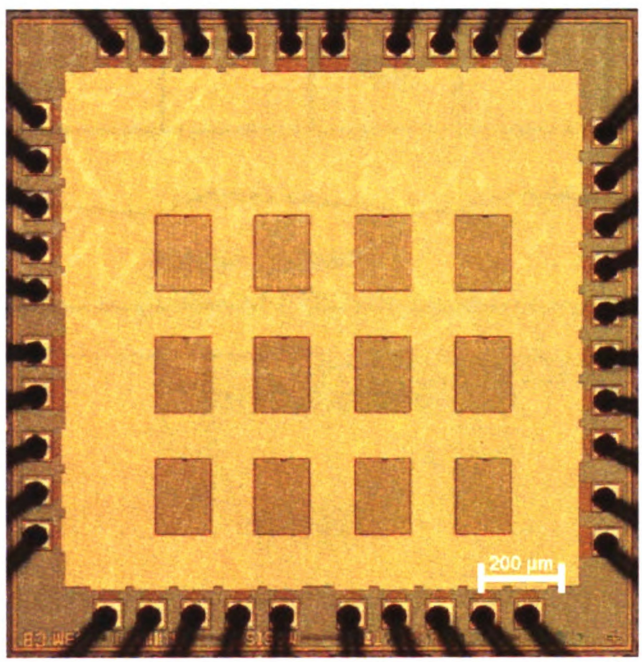

Figure 6.9 Die photograph of CMOS optical detection IC.

6.2.1 Simulation results

The optical detection CMOS chip was simulated for different values of photocurrent ranging from 10nA to 100nA. Different test points were added in the design to test different parameters of the chip. Integrator output and digital output from sigma delta ADC were verified. **Figure 6.10** shows the cadence simulation results for a 70nA photocurrent with integrator output as well as digital output from the latch. Width of the digital signal can be measured by using an off-chip digital counter. A range of discharging time at the output of integrator for a range of photocurrent from 10nA to 100nA is shown in **Figure 6.11**.

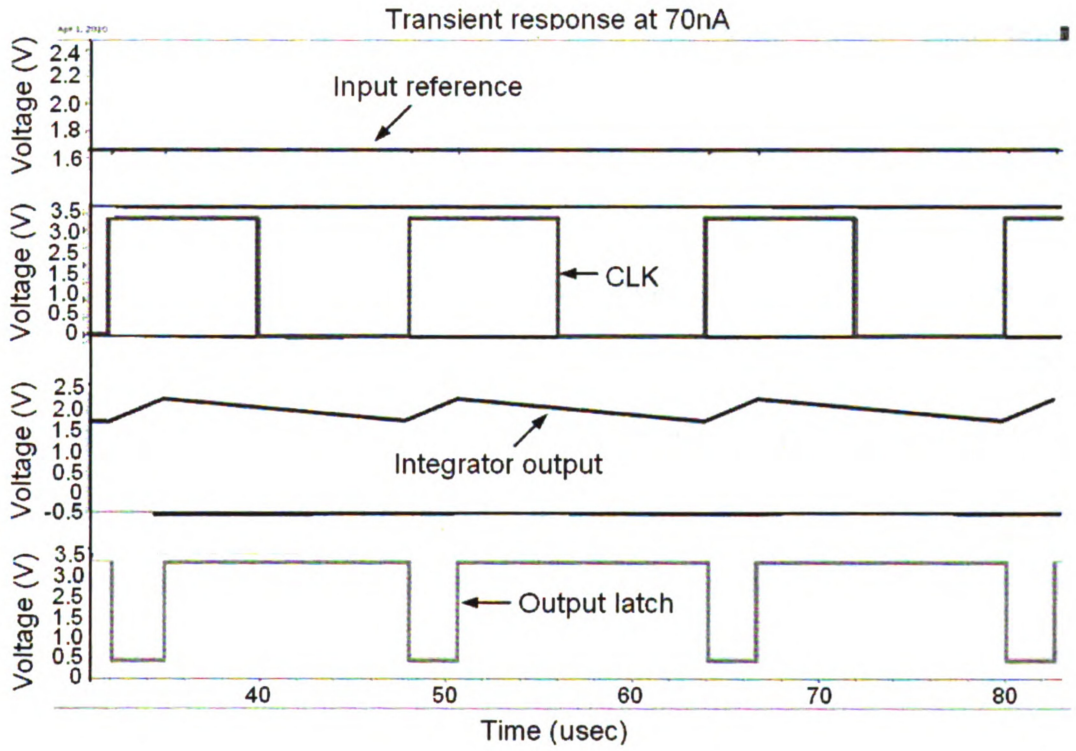

Figure 6.10. Cadence simulation of a single pixel for 70nA with integrator analog output and digital output from the comparator.

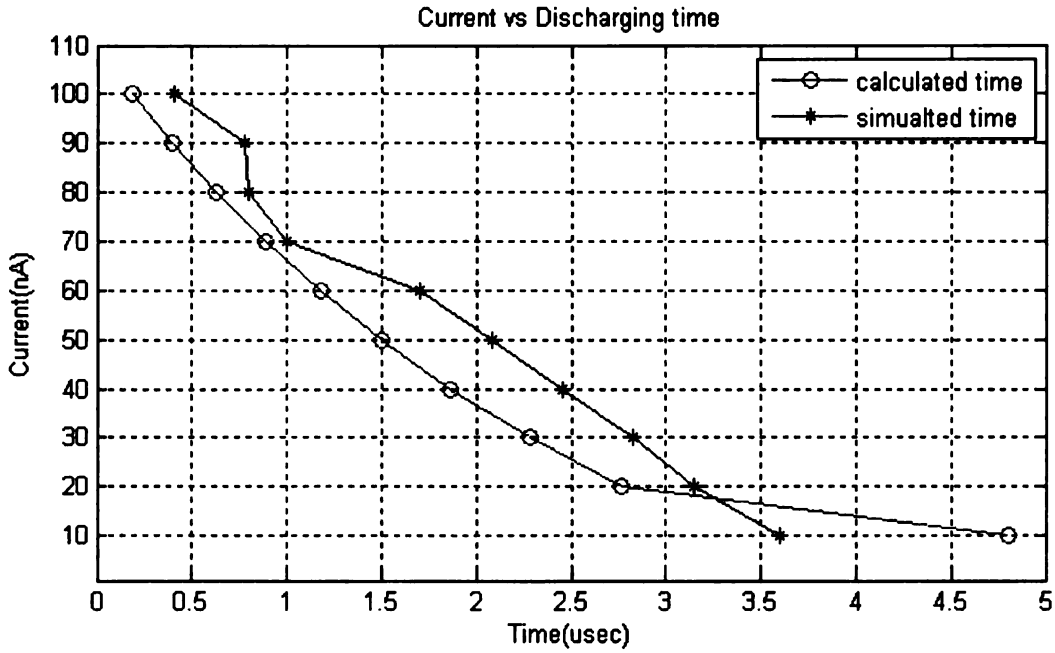

Figure 6.11. Calculated and simulated time for the discharge of photocurrent using single pixel sigma-delta ADC.

6.3 On-chip filter

6.3.1 Simulation results

To test the functionality of on-chip filter, simulations were done in MATLAB for different values of excitation and emission wavelength in the visible range of light that can be detected by the photodiode. **Figure 6.12** shows the physical model used for the simulation that contains three metal layers with the same parameters and values as dictated by the "design rule check (DRC)" rules for C5N CMOS process. These simulations were done to determine the minimum wavelength of incident light allowed to pass through the filter. **Table IV** shows the minimum and maximum values used for the three layers used in simulation which follow DRC rules of C5N process. These simulations were based on the same diffraction grating equation (2) as discussed in chapter 4.

These simulations give a digital response to show the blocking of excitation light and allowing the emission light. A plot of emitted wavelengths that were allowed to pass through the diffraction grating from three adjacent slits has been shown in **Figure 6.13** where x-axis represent the normalized location on n-well where light after passing through the filter enters into n-well to create electron-hole pair (EHP), while y-axis shows the wavelength of incident light. Different colors represent different wavelengths and data points when projected on the x-axis show the location of transmitted light falling on n-well from a series of adjacent slits s_1, s_2 and s_3. These different locations for different wavelength of light are due to the change in diffraction angle for different wavelengths of light. These simulations reveal that using the above configuration a minimum emission light that can pass through the designed configuration is 740nm, while the light with a wavelength less than 740nm is blocked. Empty regions between emission light stripes show that

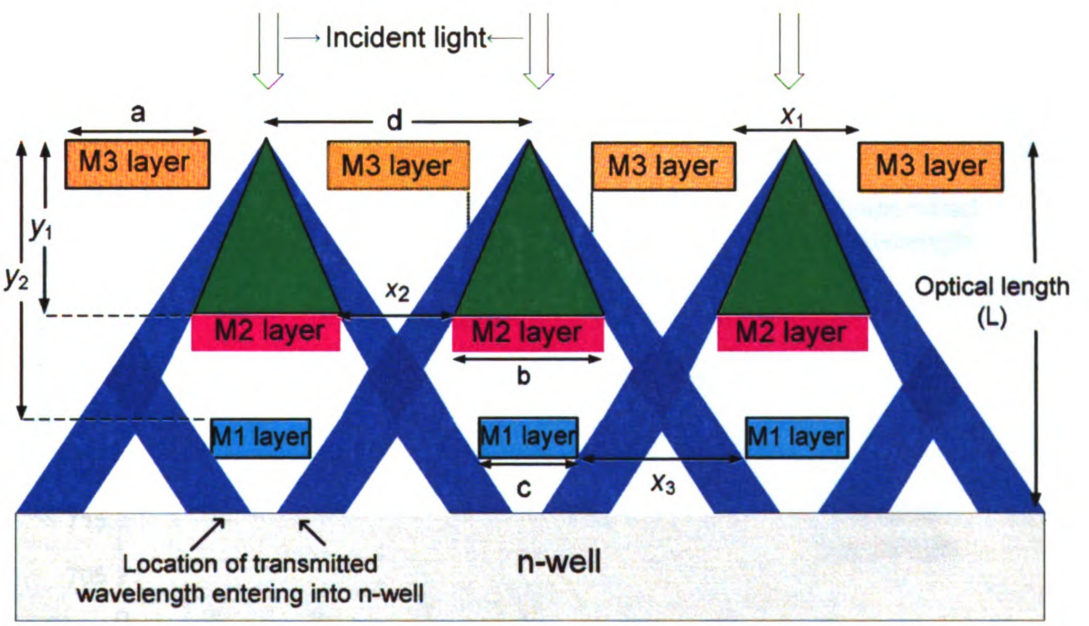

Figure 6.12 Physical model used for optical simulation in MATLAB.

light is blocked by either M2 or M1 layer stripes. **Figure 6.14** shows the digital output from the above configuration showing the wavelength range of incident light passing through it.

In addition, for other advanced CMOS process i.e. 0.18μm, 0.13 μm processes which use different number of metal layers with different separation and thickness of metal layers, this topology can be used as a band pass filter. Analysis for the effect of extra metal layers on the selectivity of filter is shown in next section.

TABLE IV. TYPES AND RANGE OF METAL LAYERS IN C5N CMOS PROCESS USED FOR MATLAB SIMULATION

Metal layer	Slit width	Slit separation
M3	0.9μm	1.5μm
M2	0.9μm (min) 1.5μm (max)	0.9μm (min) 1.2μm (max)
M1	1.2μm (min) 1.5μm (max)	0.9μm(min) 1.2μm(max)

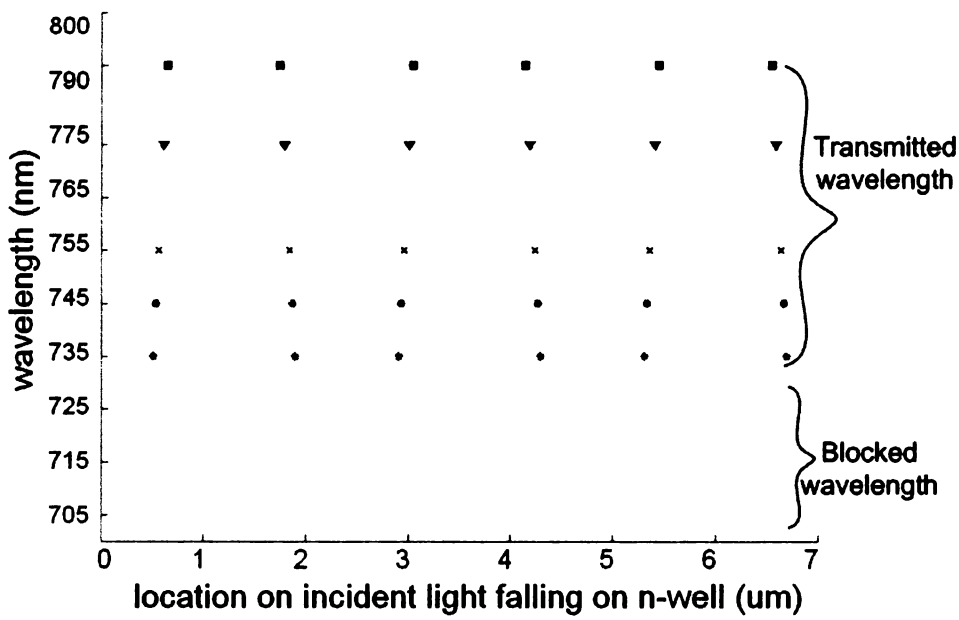

Figure 6.13. Locations of incident light of wavelength on n-well with different colors showing the light coming from different adjacent slits.

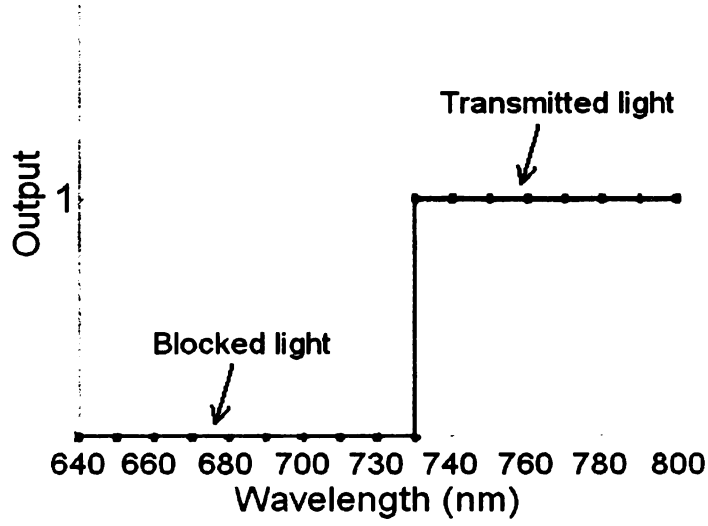

Figure 6.14. Range of incident light wavelength allowed to pass through the filter shown by a digital signal.

6.3.2 Effect of extra metal layers on the selectivity of filter

To study the effect of extra metal layers and advanced CMOS fabrication processes on the selectivity of filter, simulations were done in MATLAB. As advanced fabrication processes support more metal layers, these metal layers can be manipulated to be used as band pass filter. Placements of these metal layers select the required wavelength of light to pass through the filter. These simulations were done to determine the range of wavelength of incident light that can be allowed to pass through the filter. For these simulations, same parameters and values i.e. metal thickness, optical length and separation between metal layers as dictated by the "design rule check (DRC)" and fabrication rules for IBM 0.13μm CMRF8SF process. Table.V shows the range of values for different metal layers used for simulations. As these values for IBM 0.13μm process are different as compared to C5N process, so these metal gratings are expected to have different results using the same design and configuration. Although 8 metal layers are allowed in the IBM

0.13μm CMRF8SF process, only 4 metal layers were used i.e. M1, M2, M3, MG to make the analysis simple. Simulations were done for 3 adjacent slits s_1, s_2 and s_3 with the same size and equally spaced. **Figure 6.15** shows different locations on the n-well (x-axis) for a range of transmitted wavelength through the filter while y-axis shows the wavelength range used in simulation. These simulations were done for visible light (320nm-780nm) and it was observed that light with a wavelength range of 400nm - 530nm is allowed to pass through the filter confirming the use of filter as band pass filter as shown in **Figure 6.16**. Similarly addition of extra metal layers and their placement can be varied to change the allowed wavelength range to pass through filter and also increase the selectivity by narrowing the wavelength range of allowed light.

TABLE .V. TYPES AND RANGE OF METAL LAYERS USED IN IBM 0.13μM PROCESS FOR MATLAB SIMULATION

Metal layer	Slit width	Slit separation
MG	0.6μm (min) 1μm (max)	0.4μm (min) 0.8μm (max)
M3	0.6μm(min) 1μm(max)	0.4μm (min) 0.8μm(max)
M2	0.4μm(min) 0.6μm(max)	0.4μm(min) 0.8μm(max)
M1	0.4μm	1μm

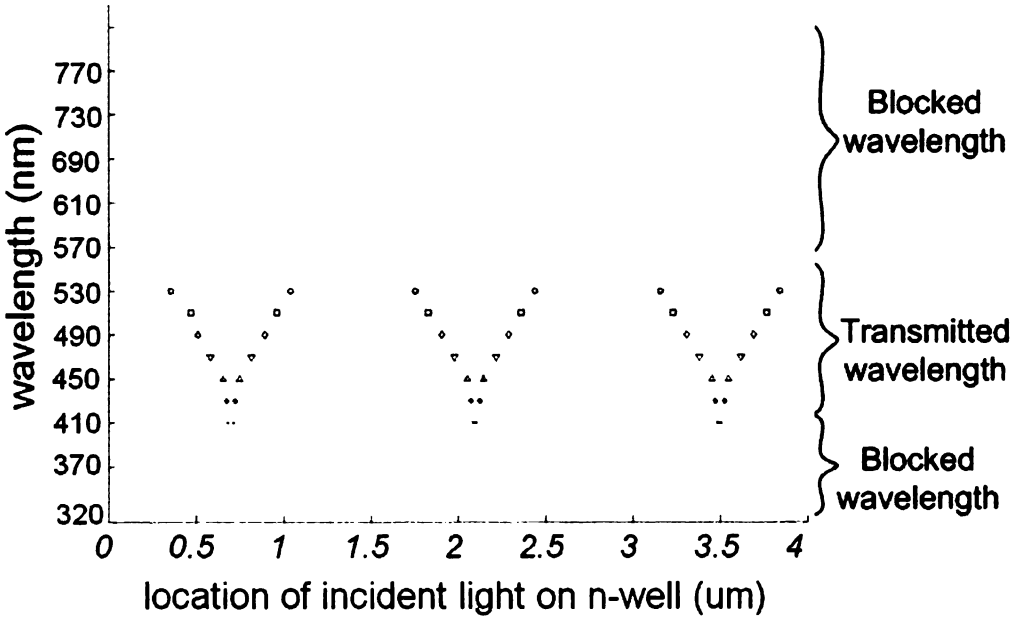

Figure 6.15. Locations of incident light of wavelength on n-well with different colors showing the light coming from different adjacent slits.

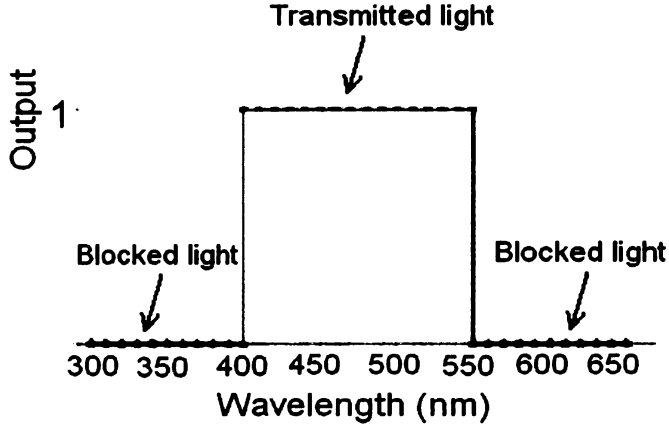

Figure 6.16. Range of incident light wavelength allowed to pass through the filter shown by a digital signal.

6.3.3 Process variations

As discussed in chapter 5 process variations also have an impact on the performance of filter, as design is inherently dependent on the fabrication process and also limited by the DRC rules. To determine the effect of process variations on the filter, filter design was simulated in MATLAB with different physical

configurations that were implemented in the CMOS chip for C5N process. In the proposed filter design for C5N process, top M3 transmission layer and M2 blocking layer have critical role in the functionality and performance of filter. So initially only M3 and M2 layer were considered for the simulation with M1 having constant slit width(x_3) of 2.4μm. A process variation of 15% was assumed for both M3 and M2 layers for the analysis. Two different cases were studied for the process variation in M3 (*a*) and M2 (b) metal layers. These process variations are underdevelopment (case 1) and overdevelopment (case 2) of both M3 and M2 layer. Table VI shows different cases that were analyzed and their effect on the light wavelength range allowed to pass through the filter. These simulations were done for a maximum wavelength of 800nm to verify the response of filter for visible light (320nm-780nm).

TABLE VI. DIFFERENT CASES FOR PROCESS VARIATIONS IN METAL WIDTHS FOR C5N PROCESS

Cases	M3 layer width	M2 layer width	Minimum transmitted wavelength
Case 1 (under-development)	a - 0.225μm	b = 1.5μm	no light
	a - 0.225μm	b +0 .225 μm	no light
	a - 0.225μm	b - 0.225 μm	**775nm**
	a - 0.225μm	b = 1.2 μm	**740nm**
	a - 0.225μm	b + 0.18 μm	no light
	a - 0.225μm	b - 0.18 μm	**635nm**
Case 2 (over-development)	a + 0.225μm	b = 1.5μm	**800nm**
	a + 0.225μm	b +0 .225 μm	no light
	a + 0.225μm	b - 0.225 μm	**680nm**
	a + 0.225μm	b = 1.2 μm	**735nm**
	a + 0.225μm	b + 0.18 μm	no light
	a + 0.225μm	b - 0.18 μm	**630nm**

6.3.4 Discussion

The simulated plot in Figure 6.11 show that a large percentage of visible light range is blocked using the configuration in Figure 6.10 as compared to the calculated values in Chapter 5. Main reasons for this blockage of incident light is due to the thickness of M3 layer that blocks maximum amount of light due to large dispersion angle for smaller wavelengths of light. This M3 layer thickness is comparable with the vertical distance between M3 and M2 layer i.e. y_1. As a result there is a difference in allowing the emission wavelength range between the calculated and simulated value, as diffraction grating equation does not include the slit thickness into account by assuming the slit thickness to be negligible as compared to slit width and slit separation.

There is a trade off between the slit width for M3 layer and M2 blocking layer width. Larger slit width allows a large range of wavelength of light to pass through it without being blocked by M3 layer thickness but at the same time it decreases the angle of dispersion. This decrease in dispersion angle decreases the selectivity of the filter as it becomes difficult for M2 layer to only block the excitation light and some wavelength of emission light is also blocked due to smaller angle deviation between lights of different wavelength.

Simulation results in Figure 6.13 show that addition of metal layers in the design increases the selectivity of the filter and can be manipulated to use it as band pass filter. Also the transmitted wavelength for both designs are different i.e. C5N and IBM 0.13µm process, because of different DRC rules and also because of

different thickness of metal layers that has a significant role in order to allow/block the incident light.

Process variations also have a prominent effect on the performance of filter. As shown in Table VI, where different cases are shown for process variation in both M3 and M2 layers. It is evident from the table that both M3 and M2 layer variation have an effect on the transmission wavelength. Another interesting fact that is given from the above table is that for both underdevelopment of M2 layer has a positive impact on the transmission wavelength for both underdevelopment and overdevelopment of M3 layer. So minimum width of M2 layer used in the design results in better efficiency and performance of filter.

The above analysis also shows the effect of using advanced CMOS process on the efficiency and performance of the proposed filter. Advanced CMOS processes use smaller feature size and extra metal layers with smaller process variations that enhances the performance of filter in terms of flexibility and selectivity. Simulation plots in Figures 6.14 and 6.15 show that, for IBM 0.13μm process, smaller feature size and more metal layers with less metal thickness allows for more wavelength transmission due to more freedom of design in slit width and slit separation and also increases the selectivity of filter as compared to the filter implemented in C5N process. Also filter implemented in IBM 0.13μm process can act as a band-pass filter as compared to C5N process that only acts as a low pass filter in visible range of light. So it is concluded that the filter designed in advanced CMOS processes i.e. 0.35μm, 0.18μm and 0.13μm would exhibit better performance as compared to the filter designed in 0.5μm CMOS process.

2.2 Conclusion

The feasibility of the VLSI realization of a programmable waveform generator and potentiostat with amperometric readout circuit with the capability of integrating on-chip electrodes is critical for the success of a multi-mode voltammetry biosensor array microsystem. In this chapter, the silicon realization of these two critical blocks i.e. waveform generator and potentiostat were characterized individually and verified with a series of experiments. Similarly realization of an optical readout circuit with integrated on-chip filter that requires no post-CMOS processing was demonstrated. Hand calculations were done for the proof of concept in utilizing the metal layers in layout as interference filter to allow specific wavelengths of light to pass through it. These calculations were verified with the simulations in MATLAB. Also it was demonstrated through simulations the effect of advanced CMOS technology on the performance and selectivity of the filter.

Chapter 7
Summary and Future Work

7.1 Summary of the contributions

Optical and electrochemical detection are considered to be the most widely used interrogation techniques for miniaturized biosensor arrays. Simultaneous implementation of these two techniques to determine multiple biomembrane processes is highly advantageous and their VLSI realization on a single chip would result in a versatile instrumentation system offering more accurate analysis and high throughput. But at the same time realization of this integration also face many challenges in terms of circuit design, fabrication of on-chip electrodes.

This dissertation provides a detailed analysis of the challenges that need to be resolved to develop an efficient on-chip instrumentation system that combines both these techniques to characterize bilipid membranes (BLP). Two separate instrumentation system for electrochemical and optical detection were developed and fabricated in C5N CMOS process. The results of this research provide a solid basis for future research in opto-electrochemical detection systems for biosensor arrays.

7.1.1 Analysis of challenges for opto-electrochemical detection system

A thorough analysis of a combined opto-electrochemical detection system to characterize membrane proteins has been done. Main challenges in the electrical design to readout both optical and electrochemical information and interference between these circuits has been discussed. Similarly issues pertaining to the integration of on-chip electrodes for electrochemical detection, filters for optical detection have been discussed. This analysis forms a solid basis to design a

combined on-chip opto-electrochemical detection system for miniaturized biosensors arrays.

7.1.2 CMOS microsystem for multimode voltammetry

An on-chip instrumentation system that supports a variety of voltammetric techniques i.e. cyclic voltammetry, linear sweep voltammetry, constant potential and normal pulse voltammetry with different scan ranges and scan rates has been developed. These techniques require different kinds of waveforms i.e. triangular waveform, linear ramp, constant potential and differential waveform for their operation. A digitally programmable waveform generator was developed to generate these waveforms. A 2 x 2 potentiostat array with amperometric readout circuit was also developed having the capability of integrating electrodes on CMOS chip.

7.1.3 Optical detection circuit

In this dissertation an optical detection circuit was also developed keeping in view the requirements of a combined opto-electrochemical detection system. A 4 x 3 pixel array was developed with n-well/p-sub photodiode and in-pixel readout based on sigma-delta ($\Sigma\Delta$) ADC. A novel technique was used for the on-chip filter that does not need any post-CMOS processing and does not provide any hindrance to electrochemical detection. The placement, width and horizontal gap between the CMOS metal layers were manipulated to create a multislit diffraction grating that passes the emission light and blocks the excitation light from the light source.

7.2 Future Work

Based on the results of this dissertation, the following suggestions for future research are made.

Although separate optical and electrochemical detection system have been developed keeping in view the requirements of combined opto-electrochemical detection system, VLSI realization of such a combined system on a monolithic chip is still a challenge. So the next step is the integration of both these techniques on a monolithic chip.

In terms of circuitry, a potential challenge for a combined opto-electrochemical system is the interference between the two readout circuits. As both these techniques are carried out at different frequencies, readout circuits for these techniques have different issues and need to work independently.

Filter performance for fluorescence detection needs to be improved for high selectivity and accuracy. Other techniques for filter design can also be considered for possible options to develop opto-electrochemical detection system.

Other electrochemical detection schemes i.e. impedance spectroscopy can also be integrated with the optical circuit for a combined instrumentation system.

Bibliography

[1] K. E. Gonsalves, C. L. Laurencin, C. R. Halberstadt, and L. S. Nair, *Biomedical Nanostructures*. NewYork: John Wiley & Sons Inc November 2007.

[2] Vo-Dinh. T and B. Cullum, "Biosensors and Biochips: Advances in Biological and Medical Diagnostics," *Fresenius J Anal Chem*, vol. 366, pp. 540-551, 2000.

[3] E. Gizeli and C. R. Lowe, "Immunosensors," *Current Opinion in Biotechnology*, vol. 7, pp. 66-79, 1996.

[4] D. J. Monk and D. R. Walt, "Optical fiber-based biosensors," *Analytical and Bioanalytical Chemistry*, vol. 379, pp. 931-945, 2004.

[5] T.Kubick, K. Bogunia-Kubik, and M. Sugisaka, "Nanotechnology on Duty in Medical Applications," *Current Pharmaceutical Biotechnology*, vol. 6, pp. 17-33, 2005.

[6] S.Kohler, S.Belkin, and R.D.Schmid, "Reporter gene bioassays in environmental analysis," *Fresenius J Anal Chem*, vol. 366, pp. 769-779, 2000.

[7] A.Reininger-Mack, H.Thielecke, and A.A.Robitzki, "3D-biohybrid systems: applications in drug screening," *Trends in biotechnology* vol. 20, pp. 56-61, 2002.

[8] W.Zhang, G.Canziani, C.Plugariu, R.Wyatt, J.Sodroski, R.Sweet, P.Kwong, W.Hendrickson, and I.Chaiken, "Conformational changes of gp120 in epitopes near the CCR5 binding site are induced by CD4 and a CD4 miniprotein mimetic," *Biochemistry*, vol. 29, pp. 9405-16, 1999.

[9] K.Yano and I.Karube, "Molecularly imprinted polymers for biosensor applications," *Trends Anal. Chem*, vol. 18, pp. 199-204, 1999.

[10] G. J. Cotton, B.Ayres, R.Xu, and T.W.Muir, "Insertion of a synthetic peptide into a recombinant protein framework: a protein biosensor " *Journal of the American Chemical Society* vol. 121, pp. 1100-1101 1999.

[11] R. F. Costello, I. R. Peterson, J. Heptinstall, and D. J. Walton, "Improved gel-protected bilayers," *Biosensors & Bioelectronics*, vol. 14, pp. 265-271, 1999.

[12] J. J. Ramsden, "Biomimetic protein immobilization using lipid bilayers," *Biosensors & Bioelectronics*, vol. 13, pp. 593-598, 1998.

[13] J. M. Kohler, A. Csaki, J. Reichert, R. Moller, W. Straube, and W. Fritzsche, "Selective labeling of oligonucleotide monolayers by metallic nanobeads for fast optical readout of DNA-chips," *Sensors and Actuators B Chem*, vol. 76, pp. 166-172, 2001.

[14] S.S.Pathak and H.F.Savelkoul, "Biosensors in immunology: the story so far," *Immunology Today*, vol. 18, pp. 464-467, 1997.

[15] L. D. Stefano, P. Arcari, A. Lamberti, C. Sanges, L. Rotiroti, I. Rea, and I. Rendina, "DNA Optical Detection Based on Porous Silicon Technology:from Biosensors to Biochips," *Sensors* vol. 7, pp. 214-221, 2007.

[16] T. Vo-Dinh, "SERS chemical sensors and biosensors: new tools for environmental and biological analysis," *Sensors and Actuators B Chem*, vol. 29, pp. 183-189, 1995.

[17] J. Dostálek and W. Knoll, "Biosensors based on surface plasmon-enhanced fluorescence spectroscopy," *Biointerphases*, vol. 3, pp. 12-22, 2008.

[18] V. Sanz, S. d. Marcos, and J. Galban, "A reagentless optical biosensor based on the intrinsic absorption properties of peroxidase," *Biosensors & Bioelectronics*, vol. 22, pp. 956-964, 2007.

[19] J. Zhang, Y. Huang, N. Trombly, C. Yang, and A. Mason, "Electrochemical Array Microsystem with Integrated Potentiostat," presented at IEEE Int.Conf. on Sensors, Irving CA, 2005.

[20] J. Wang, X. J. Zhang, and M. Prakash, "Glucose microsensors based on carbon paste enzyme electrodes modified with cupric hexacyanoferrate," *Analytica Chimica Acta*, vol. 395, pp. 11-16, 1999.

[21] J. Kulys, "The carbon paste electrode encrusted with a microreactor as glucose biosensor," *Biosensors & Bioelectronics*, vol. 14, pp. 473-479, 1999.

[22] V. G. Andreou and D. P. Nikolelis, "Electrochemical transduction of interactions of aflatoxin Ml with bilayer lipid membranes (BLMs) for the construction of one-shot sensors " *Sensors and Actuators B Chem*, vol. 41, pp. 213-216, 1997.

[23] C. Yang, Y. Huang, B. L. Hassler, R. M. Worden, and A. J. Mason, "Amperometric Electrochemical Microsystem for a Miniaturized Protein Biosensor Array," presented at IEEE Biomedical Circ. Systems, 2009.

[24] M. Breten, T. Lehmann, and E. Braun, "Integrating data converters for picoampere currents from electrochemical transducers," presented at IEEE International Symposium on Circuits and Systems, Geneva, 2000.

[25] A. Hassibi and T. H. Lee, "A Programmable Electrochemical Biosensor Array in 0.18μm Standard CMOS," presented at International Symp. Solid-State Circuits, 2005.

[26] P. Kim, N. Kohli, B. Hassler, N. Dotson, A. Mason, R. M. Worden, and R. Ofoli, "An Electrochemical Interface for Integrated Biosensors," presented at IEEE Int. Conf. on Sensors, Toronto, Canada, 2003.

[27] C. Yang, Y. Huang, B. L. Hassler, R. M. Worden, and A. J. Mason, "Amperometric Electrochemical Microsystem for a Miniaturized Protein Biosensor Array," *IEEE Trans. Biomedical Circ. Systems*, vol. 3, pp. 160-168, 2009.

[28] X. Yang, C. Shi, R. E. Holmlin, S. O. Kelley, M. G. Hill, D. M. Crothers, and J. K. Barton, "Electrochemical Microsensors for DNA Mutation Detection," *Digest Solid-State Sensor, Actuator and Microsystems Workshop*, pp. 118-121, 2002.

[29] E. Bakker, and M. Telting-Diaz, "Electrochemical Sensors," *Anal. Chem.*, vol. 74, pp. 2781-2800, 2002.

[30] Y.-H. Zheng, T.-C. Hua, and F. Xu, "A Thermal Biosensor Based on Enzyme Reaction," presented at IEEE-Engineering in Medicine and Biology(EMBS), Shanghai,China, 2005.

[31] J. E. Kohn and K. W. Plaxco, "Engineering a signal transduction mechanism for protein-based biosensors," presented at Proc of National Academy of Sciences(PNAS), 2005.

[32] S. Song, Hui Xu, and C. Fan, "Potential diagnostic applications of biosensors: current and future directions," *International Journal of Nanomedicine*, vol. 1, pp. 433-440, 2006.

[33] G. S. Bang, S. Cho, and B. G. Kim, "A novel electrochemical detection method for aptamer biosensors," *Biosensors & Bioelectronics*, vol. 21, pp. 863-870, 2005.

[34] K. Ikebukuro, C. Kiyohara, and K. Sode, "Novel electrochemical sensor system for protein using the aptamers in sandwich manner," *Biosensors & Bioelectronics*, vol. 20, pp. 2168-2172, 2005.

[35] A. E. Radi, J. L. A. Sanchez, E. Baldrich, and C. K. O'Sullivan, "Reusable impedimetric aptasensor," *Analytical Chemistry(ACS)*, vol. 77, pp. 6320-6323, 2005.

[36] K. Maehashi, T. Katsura, K. Kerman, Y. Takamura, K. Matsumoto, and E. Tamiya, "Label-free protein biosensor based on aptamer-modified carbon nanotube field-effect transistors," *Analytical Chemistry(ACS)*, vol. 79, pp. 782-787, 2007.

[37] J. A. Hansen, J. Wang, A. N. Kawde, Y. Xiang, K. V. Gothelf, and G. Collins, "Quantum-dot/aptamer-based ultrasensitive multi-analyte electrochemical biosensor," *Journal of the American Chemical Society(JACS)*, vol. 128, pp. 2228-2229, 2006.

[38] R. Turpeinen, M. Virta, and M. Haggblom, "Analysis of Arsenic Bioavailability in Contaminated Soils," *Environmental Toxilogy and Chemistry(ET&C)*, vol. 22, pp. 1-6, 2003.

[39] G. Marrazza, I. Chianella, and M. Mascini, "Disposable DNA electrochemical sensor for hybridization detection " *Biosensors & Bioelectronics*, vol. 14, pp. 43-51, 1999.

[40] J. Wang, X. Cai, G. Rivas, H. Shiraishi, and N. Dortha, "Nucleic acid immobilization, recognition and detection at chronoamperometric DNA chips," *Biosensors & Bioelectronics*, vol. 12, pp. 587-599, 1997.

[41] M. P. Marco and D.Barcelo, "Environmental applications of analytical biosensros," *Meas. Sci. Tech*, vol. 7, pp. 1547-1562, 1996.

[42] P. Yin, C. J. Burns, P. D. J. Osman, and B. A. Cornell, "A tethered bilayer sensor containing alamethicin channels and its detection of amiloride based inhibitors," *Biosensors & Bioelectronics*, vol. 18, pp. 389-397, 2003.

[43] M. Trojanowicz, "Miniaturized Biochemical Sensing Devices Based on Planar Bilayer Lipid Membranes," *Fresenius J Anal Chem*, vol. 371, pp. 246-260, 2001.

[44] C. Yang, D. Rairigh, and A. Mason, "On-Chip Electrochemical Impedance Spectroscopy for Biosensor Arrays," presented at IEEE Int. Conf. on Sensors, Daejeon, Korea, 2006.

[45] B. Jang and A. Hassibi, "Biosensor systems in standard CMOS processes: Fact or fiction?," presented at IEEE Symp on Industrial Electronics(ISIE), 2008.

[46] M. Schienle, C. Paulus, A. Frey, F. Hofmann, B. Holzapfl, P. Schindler-Bauer, and R. Thewes, "A Fully Electronic DNA Sensor with 128 Positions and In-Pixel A/D Conversion," *J. Solid-State Circuits*, vol. 39, pp. 2438-2445, 2004.

[47] J. Ohta, *Smart CMOS Image Sensors and Applications*: Barnes & Noble, Sep 2007.

[48] C. Yi, Q. Zhang, C.-W. Li, Y. Yang, J. Zhao, and M. Yang, "Optical and electrochemical detection techniques for cell-based microfluidic systems," *Analytical and Bioanalytical Chemistry* vol. 384, pp. 1259-1268, 2006.

[49] P. Abbyad, W. Childs, X. Shi, and S. G. Boxer, "Dynamic Stokes shift in green fluorescent protein variants," *National Academy of Sciences(PNAS)*, vol. 104, pp. 20189-20194, 2007.

[50] A. Bandyopadhyay, G. Mulliken, G. Cauwenberghs, N. Thakor, "VLSI Potentiostat for Distributed Electrochemical Neural Recording," *IEEE Int. Sym. on Circ. and Systems*, vol. 2, pp. 740-743, 2002.

[51] A. Frey, M. Jenkner, M. Schienle, C. Paulus, B. Holzapfl, P. Schindler-Bauer, F. Hofmann, D. Kuhlmeier, J. Krause, J. Albers, W. Gumbrecht, D. Schmitt-Landsiedel, and R. Thewes, "Design of an integrated potentiostat circuit for CMOS bio sensor chips," presented at IEEE International SymposiumCircuits and Systems, Bangkok, Thailand, 2003.

[52] R. Genov, M. Stanacevic, M. Naware, G. Cauwenberghs, and N. Thakor, "VLSI Multi-Channel Track-and-Hold Potentiostat," presented at Microtechnologies for the New Millennium 2003, Proc. SPIE, 2003.

[53] R. G. Kakerow, H. Kappert, E. Spiegel, and Y. Manoli, "Low-Power Single-Chip CMOS Potentiostat," *Int. Conf. Solid-State Sensors and Actuators (Transducers)*, vol. 1, pp. 142-145, 1995.

[54] E. Katz, I. Willner, "Probing Biomolecular Interactions at Conductive and Semiconductive Surfaces by Impedance Spectroscopy: Routes to Impedimetric Immunosensors, DNA-Sensors, and Enzyme Biosensors," *Electroanalysis*, vol. 15, pp. 913-947, 2003.

[55] S. M. Martin, F. H. Gebara, T. D. Strong, and R. B. Brown, "A Low-Voltage, Chemical Sensor Interface for Systems-On-Chip: The Fully-Differential Potentiostat," presented at IEEE Int. Symp. Circuits and Systems, Vancouver, Canada, 2004.

[56] R. Matos, L. Angnes, and C. L. do Lago, "Development of a four-channel potentiostat for amperometric detection in flow injection analysis," *Instrumentation Science & Technology*, vol. 26, pp. 451-459, 1998.

[57] H. S. Narula and J. G. Harris, "Integrated VLSI Potentiostat for Cyclic Voltametry in Electrolytic Reactions," presented at IEEE Computer Society Symp. on VLSI, 2004.

[58] M. Naware, A. Rege, R. Genov, M. Stanacevic, G. Cauwenberghs, and N. Thakor, "Integrated Multi-Electrode Fluidic Nitric-Oxide Sensor and VLSI Potentiostat Array," presented at IEEE Int. Symp. Circuits and Systems, Vancouver, Canada, 2004.

[59] R. J. Reay, S.P. Kounaves, and G.T.A. Kovacs, "An Integrated CMOS Potentiostat for Miniaturized Electroanalytical Instrumentation," *Proc. Inter. Solid-State Circuits Conf.*, pp. 162 - 163, 1994.

[60] R. F. B. Turner, D. J. Harrison, and H. P. Baltes, "A CMOS Potentiostat for Amperometric Chemical Sensors," *IEEE J.Solid-State Circuits*, vol. 22, pp. 473-478, 1987.

[61] Ratnakumar. B. V, Smart. M. C, and S. S, "Electrochemical Impedance Spectroscopy and Its Applications to Lithium Ion Cells," presented at Annual Battery Conf. Appl. Adv, CA, USA, 2002.

[62] R. Sanders and H. C. Gererritsen, "Fluorescence lifetime imaging of free calcium in single cells," *Bioimaging*, pp. 1331-138, 1994.

[63] D. Elson, S. Webb, J. Siegel, K. Suhling, D. Davis, J. Lever, D. Phillips, A. Wallace, and P. French, "Biomedical applications of fluorescence lifetime imaging," *Opt. Photon. News*, pp. 27-32, 2002.

[64] K. Dowling, M. J. Dayel, S. Hyde, P. French, M. J. Lever, and J. D. Hares, "High resolution time-domain fluorescence lifetime imaging for biomedical applications," *Journal of Modern Optics*, vol. 2, pp. 199-209, 1999.

[65] M. Elangovan, R. N. Day, and A. Periasamy, "Nanosecond fluorescence resonance energy transfer-fluorescence lifetime imaging microscopy to localize the protein interactions in a single living cell," *Journal of Microscopy*, vol. 205, pp. 3-14, 2002.

[66] J. R. Lakowicz, "Emerging Biomedical Applications of Time-Resolved Fluorescence Spectroscopy " in *Topics in Fluorescence Spectroscopy*, vol. 4: Springer US, 2006, pp. 1-19.

[67] C. Dongre, R. Dekker, H. J. W. M. Hoekstra, D. Nolli, R. M-Vazquez, R. Osellame, G. Cerullo, G. A. J. Besselink, and M. Pollnau, "Fluorescence sensing with femtosecond laser written waveguides in a capillary electrophoresis chip for monitoring molecular separation," presented at European Conference On Integrated Optics (ECIO), Eindhoven, The Netherlands, 2008.

[68] L. Brand, C. Eggeling, C. Zander, K. H. Drexhage, and C. A. M. Seidel, "Single-Molecule Identification of Coumarin-120 by Time-Resolved Fluorescence Detection: Comparison of One- and Two-Photon Excitation in Solution," *The Journal of Physical Chemistry*, vol. 101, pp. 4313-4321, 1997.

[69] J. Malicka, I. Gryczynski, B. P. Maliwal, J. Fang, and J. R. Lakowicz, "Fluorescence Spectral Properties of Cyanine Dye Labeled DNA Near Metallic Silver Particles," *Analytical Biochemistry*, vol. 317, pp. 136-146, 2003.

[70] C. Shi, H. Gu, and C. Ma, "An aptamer-based fluorescent biosensor for potassium ion detection using a pyrene-labeled molecular beacon " *Analytical Biochemistry*, vol. 400, pp. 99-102, 2010.

[71] H. Harma, T. Soukka, and T. Lovgren, "Europium Nanoparticles and Time-resolved Fluorescence for Ultrasensitive Detection of Prostate-specific Antigen " *Clinical Chemistry*, vol. 47, pp. 561-568, 2001.

[72] Soares. A and Perry. R, "A Two-Color CMOS Optical Detector Circuit," presented at Proceedings of IEEE Southeast Conf, 2007.

[73] Ardeshirpour.Y, Deem.M.J, and Shirani.S, "2-D CMONS Based Image Sensor System for Fluorescent Detection," presented at Proceedings of Canadian Conference on Electrical and Computer Engineer, 2004.

[74] Darain. F, Yager. P, Gan. K. L, and S. C. Tjin, "On-chip detection of myoglobin based on fluorescence," *Biosensors & Bioelectronics*, vol. 24, pp. 1744-1750, 2009.

[75] J. L. Fu, Q. Fang, T. Zhang, X. H. Jin, and Z. L. Fang, "Laser-Induced Fluorescence Detection System for Microfluidic Chips Based on an Orthogonal Optical Arrangement," *Analytical Chemistry(ACS)*, vol. 78, pp. 3827-3834, 2006.

[76] Zourob.M, Mohr.S, Brown.B.J.T, Fielden.P.R, McDonnell.M.B, and Goddard.N.J, "Bacteria detection using disposable optical leaky waveguide sensors " *Biosensors & Bioelectronics*, vol. 21, pp. 293-302, 2002.

[77] M. Beiderman, T. Tam, A. Fish, G. A. Jullien, and O. Yadid-Pecht, "A Low-Light CMOS Contact Imager With an Emission Filter for Biosensing Applications," presented at IEEE Biomedical Circ. Systems, 2008.

[78] T. Huang, S. Sorgenfrei, K. L. Shepard, P. Gong, and R. Levicky, "A CMOS Array Sensor for Sub-800-ps Time-Resolved Fluorescence Detection," presented at IEEE Custom Intergrated Circuits Conference 2007.

[79] B. Jang, P. Cao, A. Chevalier, A. Ellington, and A. Hassibi, "A CMOS Fluorescent-Based Biosensor Microarray," presented at IEEE International Solid-State Circuits Conference 2009.

[80] M. L. Simpson, G. S. Sayler, G. Patterson, D. E. Nivens, E. K. Bolton, J. M. Rochelle, J. C. Arnott, B. N. Applegate, S. Ripp, and M. A. Guillorn, "An integrated CMOS microluminometer for low-level luminescence sensing in the bioluminescent bioreporter intergated circuit," *Sensors and Actuators*, pp. 134-140, 2001.

[81] R. A. Yotter and D. M. Wilson, "A Review of Photodetectors for Sensing Light-Emitting Reporters in Biological Systems," *IEEE SENSORS JOURNAL*, vol. 3, pp. 60, 2003.

[82] C. Niclass, M. Sergio, and E. Charbon, "A single photon Avalanche Diode Array fabricated in Deep-submicron CMOS Technology," presented at Proc of Design, Automation and Test in Europe, 2006.

[83] T.-C. D. Huang, S. Sorgenfrei, P. Gong, R. Levicky, and K. L. Shepard, "A 0.18- m CMOS Array Sensor for Integrated Time-Resolved Fluorescence Detection," *IEEE Journal of Solid State Circuits (JSSC)*, vol. 44, pp. 1644-1654, 2009.

[84] S. Yoshihara, Y. Nitta, M. Kikuchi, K. Koseki, Y. Ito, Y. Inada, S. Kuramochi, H. Wakabayashi, M. Okano, H. Kuriyama, J. Inutsuka, A. Tajima, T. Nakajima, Y. Kudoh, F. Koga, Y. Kasagi, S. Watanabe, and T. Nomoto, "A 1/1.8-inch 6.4 MPixel 60 frames/s CMOS Image Sensor With Seamless Mode Change," *IEEE J. Solid State Circuits*, vol. 41, pp. 2998-3006, 2006.

[85] M. Mori, M. Katsuno, S. Kasuga, T. Murata, and T. Yamaguchi, "A 1/4in 2M Pixel CMOS Image Sensor with 1.75 Transistor/Pixel," presented at IEEE International Solid-State Circuits Conference, 2004.

[86] D. Yang, A. E. Gamal, B. Fowler, and H. Tian, "A 640 x 512 CMOS Image Sensor with Ultrawide Dynamic Range Floating-Point Pixel-Level ADC," *IEEE J. Solid State Circuits*, vol. 34, pp. 1821-1834, 1999.

[87] Chediak. J. A, L. Z., and S. J, "Heterogeneous integration of CdS filters with GaN LEDs for fluorescence detection microsystems," *Sensor and Actuators A*, 2003.

[88] Webster. J. R, Burns. M. A, Burke. D. T, and M. C. H, "Electrocphoresis system with integrtaed on-chip fluorescence detection," presented at IEEE MEMS Miyazaki, Japan, 2000.

[89] Shuai. Y, Banerjee. A, Klotzkin. D, and P. I, "On-chip Fluorescence Detection using Organic Thin Film Devices for a Disposable Lab-on-a-chip," presented at IEEE Sensors, 2008.

[90] Thrush.E, Levi.O, Cook.L.J, Deich.J, Kurtz.A, Smith.S.J, Moerner.W.E, and H. Jr.J.S, "Monolithically integrated semiconductor fluorescence sensor for microfluidic applications," *Sensors and Actuators B Chem*, vol. 105, pp. 393-399, 2005.

[91] P. Arguel, J. Valentin, S. Fourment, F. Lzoes-Dupuy, G. Sarrabayrouse, S. Bonnefont, Y. Jourlin, S. Reynaud, N. Destouches, A.V. Tishchenko, and J. Jay, "A monolithic optical phase-shift detector on Silicon," *IEEE Sensors*, vol. 5, pp. 1305-1309, 2005.

[92] Dai. C-L, Chen. H-L, Yu. L-B, Lin. C-H, and Chang. P-Z, "Design and fabrication of CMOS optical modulator " *Sensors and Actuators A*, vol. 95, pp. 69-74, 2001.

[93] P. B. Catrysse, W. Suh, S. Fan, and M. Peeters, "One-mode model for patterned metal layers inside integrated color pixels," *Optics letters*, vol. 29, pp. 974-976, 2004.

[94] G. Patounakis, K. L. Shepard, and R. Levicky, "Active CMOS Array Sensor for Time-Resolved Fluorescence Detection," *IEEE J. Solid State Circuits*, vol. 41, pp. 2521-2530, 2006.

[95] Ta-chien, D. Huang, S. Sorgenfrei, P. Gong, R. Levicky, and K. L. Shepard, "A 0.18-um CMOS Array Sensor for Integrated Time-Resolved Fluorescence Detection," *IEEE J. Solid State Circuits*, vol. 44, pp. 1644-1654, 2009.

[96] B. R. Rae, K. R. Muir, D. Renshaw, R. K. Henderson, J. Girkin, Z. Gong, J. McKendry, E. Gu, and M. D. Dawson, "A Vertically Integrated CMOS Micro-System for Time- Resolved Fluorescence Analysis," presented at IEEE Biomedical Circ. Systems, Beijing, 2009.

[97] J. A. Richardson, L. A. Grant, and R. K. Henderson, "Low Dark Count Single-Photon Avalanche Diode Structure Compatible With Standard Nanometer Scale CMOS Technology," *IEEE Photonics Technology Letters*, vol. 21, pp. 1020-1022, 2009.

[98] D. Stoppa, D. Mosconi, L. Pancheri, and L. Gonzo, "Single-Photon Avalanche Diode CMOS Sensor for Time-Resolved Fluorescence Measurements," *IEEE Sensors journal*, vol. 9, pp. 1084-1090, 2009.

[99] Mason.A, H. Yue, Y. Chao, and Z. J, "Amperometric Readout and Electrode Array Chip for Bioelectrochemical Sensors," presented at IEEE. Int Symposium on Circ. and Systems (ISCAS), 2007.

[100] Hintsche.R, Albers.J, Bernt.H, and Eder.A, "Multiplexing of Microelectrode Arrays in Voltammetric Measurements," *Electroanalysis*, vol. 12, pp. 660-665, 2000.

[101] Chan.F-L, C. W-Y, K. L-M, L. C-H, W. S-W, Y. Y-S, and L. M-S-C, "An Electrochemical dopamine sensor with a CMOS detection circuit," *Journal of Micromechanics and Microengineering*, vol. 18, 2008.

[102] M. Nazari, H. and R. Genov, "A fully differential CMOS potentiostat," *IEEE Int. Sym. on Circ. and Systems*, pp. 2177-2180, 2009.

[103] C. Yang, S. R. Jadhav, R. M. Worden, and A. J. Mason, "Compact Low Power Impedance-to-Digital Converter for Sensor Array Microsystems," *IEEE J. Solid State Circuits*, vol. 44, pp. 2844-2855, 2009.

[104] A. Manickam, A. Chevalier, M. McDermott, A. Ellington, and A. Hassibi, "A CMOS Electrochemical Impedance Spectroscopy Biosensor Array for label-free Biomolecular detection " presented at IEEE Int. Solid State Circuits Conference(ISSCC), 2010.

[105] F. Heer, W. Franks, A. Blau, S. Taschin, C. Ziegler, A. Hierlemann, and H. Baltes, "CMOS microelectrode array for the monitoring of electrogenic cells," *Biosensors & Bioelectronics*, vol. 20, pp. 358-366, 2004.

[106] A. Chovin, P. Garrigue, P. Vinatier, and N. Sojic, "Development of an Ordered Array of Optoelectrochemical Individually Readable Sensors with Submicrometer Dimensions: Application to Remote Electrochemiluminescence Imaging," *Anal. Chem.*, vol. 76, pp. 357-364, 2004.

[107] L.-C. Chen and K.-C. Ho, "Multimode optoelectrochemical detection of cysteine based on an electrochromic Prussian blue electrode," *Sens. Actuators B, Chem.*, vol. 130, pp. 418-424, 2008.

[108] G. Singh, D. Moore, and R. F. Saraf, "Localized Electrochemistry on a 10um Spot on a Monolithic Large Electrode: An Avenue for Electrochemical Microarray Analysis," *Anal. Chem.*, vol. 81, pp. 6055-6060, 2009.

[109] T. Tokuda, K. Tanaka, M. Matsuo, K. Kagawa, M. Nunoshita, and J. Ohta, "Optical and electrochemical dual-image CMOS sensor for on-chip biomolecular sensing applications," *Sensors and Actuators* pp. 315-322, 2007.

[110] A. Agah, A. Hassibi, J. D. Plummer, and P. B. Griffin, "Design requirements for integrated biosensor arrays," presented at Proc of the SPIE, 2005.

[111] C. Yang, "Impedance Extraction Microsystem for nanostrucured electrochemical sensor arrays," in *Electrical and Computer Engineering*, vol. PhD. East Lansing: Michigan State University, 2008, pp. 155.

[112] G.E.Hack, "Binary up/down counter," *IBM technical Disclosure Bulletin*, vol. 24, pp. 4399-4400, 1982.

[113] X. D. Lu and P. C. Treleaven, "A special-purpose VLSI chip:A dynamic pipeline up-down counter," *J. Microprocess. Microprogram*, vol. 10, pp. 1-10, 1982.

[114] C. Yang, Y. Huang, B. L. Hassler, R. M. Worden, and A. J. Mason, "Amperometric Electrochemical Microsystem for a Miniaturized Protein Biosensor Array," *Proc of IEEE Biomedical Circ. Systems*, vol. 3, pp. 160-168, 2009.

[115] X. Liu, "Amperometric readout circuit," in *Electrical and Computer Engineering*, vol. M.S. East Lansing: Michigan State University, 2009.

[116] C. C. Enz and G. C. Temes, "Circuit techniques for reducing the effects of op-amp imperfections: autozeroing, correlated double sampling, and chopper stabilization," *Proceedings of the IEEE*, vol. 84, pp. 1584-1614, 1996.

[117] H. Eltoukhy, K. Salama, and A. E. Gamal, "A 0.18μm CMOS Bioluminescence Detection Lab-on-Chip," *IEEE J. Solid State Circuits*, vol. 41, 2006.

[118] B. Fowler, A. E. Gamal, and D. Yang, "Techniques for Pixel Level Analog to Digital Conversion," *Proc of SPIE conference on Infrared Readout Electronics*, vol. 3360, 1998.

[119] S.-H. Huang and W.-Z. Chen, "A 10-Gbps CMOS Single Chip Optical Reciever with 2-D Meshed Spatially-Modulated Light Detector," *Proc of IEEE Custom Intergrated Circuits Conference (CICC)* vol. 6, pp. 129-132, 2009.

[120] L. Baker, and Boyce, *CMOS Circuit Design, Layout, and Simulation*: IEEE Press, 1998.

[121] M. Dandin, P. Abshire, and E. Smela, "Optical filtering technologies for integrated fluorescence sensors," *Lab on a Chip* vol. 7, pp. 955-977, 2007.